MIT Open Access Articles

Reduced Basis Approximation and a Posteriori Error Estimation for the Parametrized Unsteady Boussinesq Equations

REDUCED BASIS APPROXIMATION AND A POSTERIORI ERROR ESTIMATION FOR THE PARAMETRIZED UNSTEADY BOUSSINESQ EQUATIONS

DAVID J. KNEZEVIC

Department of Mechanical Engineering and Center for Computational Engineering,
Massachusetts Institute of Technology, 77 Massachusetts Ave, Cambridge, MA 02139 USA
dknez@mit.edu

NGOC-CUONG NGUYEN

Department of Mechanical Engineering and Center for Computational Engineering,
Massachusetts Institute of Technology, 77 Massachusetts Ave, Cambridge, MA 02139 USA
cuongng@mit.edu

ANTHONY T. PATERA*

Department of Mechanical Engineering and Center for Computational Engineering,
Massachusetts Institute of Technology
Room 3-266, 77 Massachusetts Ave, Cambridge, MA 02139 USA
patera@mit.edu

In this paper we present reduced basis approximations and associated rigorous *a posteriori* error bounds for the parametrized unsteady Boussinesq equations. The essential ingredients are Galerkin projection onto a low-dimensional space associated with a smooth parametric manifold — to provide dimension reduction; an efficient POD-Greedy sampling method for identification of optimal and numerically stable approximations — to yield rapid convergence; accurate (Online) calculation of the solution-dependent stability factor by the Successive Constraint Method — to quantify the growth of perturbations/residuals in time; rigorous *a posteriori* bounds for the errors in the reduced basis approximation and associated outputs — to provide *certainty* in our predictions; and an Offline-Online computational decomposition strategy for our reduced basis approximation and associated error bound — to minimize marginal cost and hence achieve high performance in the real-time and many-query contexts. The method is applied to a transient natural convection problem in a two-dimensional "complex" enclosure — a square with a small rectangle cut-out — parametrized by Grashof number and orientation with respect to gravity. Numerical results indicate that the reduced basis approximation converges rapidly and that furthermore the (inexpensive) rigorous *a posteriori* error bounds remain practicable for parameter domains and final times of physical interest.

Keywords: Boussinesq equations; stability; reduced order model; reduced basis approxi-

---

*Corresponding author.

2   *D. J. Knezevic, N. C. Nguyen, A. T. Patera*

mation; a posteriori error estimation; error bounds; POD-Greedy sampling; offline-online procedure; successive constraint method; real-time computation

1. Introduction

The analysis of unsteady natural convection heat transfer and fluid flow governed by the Boussinesq equations (obtained from the Boussinesq approximation of the Navier-Stokes and energy equations) has received considerable attention for many years [25, 30, 57]. Natural convection flows are relevant in many engineering applications including thermal insulation, solar energy systems, reactor cooling systems, ground-water pollution, ocean modeling, and materials processing. In these, and many other applications, it is crucial to understand the unsteady flow and transport over a range of (dimensionless) parameters such as the Grashof number or Rayleigh number, the Prandtl number, and (say) gravity orientation — typically a very computationally intensive prospect [4, 19, 38]. In this paper, we explore one fashion in which to accelerate parameter-space exploration in the many-query and also real-time contexts — *reduced order models*.

It has been observed for many nonlinear partial differential equations that the solution manifold is of low dimension; in the natural convection context, the Lorenz model [42] is the classical reference. This feature can be exploited in a reduced order model. The reduced order model can often capture the system behavior accurately; examples from fluid dynamics include [10, 12, 13, 24, 27, 31–33, 35]. Furthermore, at least for systems with only quadratic nonlinearities — such as the Boussinesq equations — the reduced order model can be significantly *less costly* than classical discretization techniques such as the finite element method. However, none of the earlier examples of reduced order models for the unsteady incompressible Navier-Stokes and Boussinesq equations [7, 10, 13, 23, 24, 31–34] is endowed with practicable and rigorous error bounds.

The *certified* reduced basis method — which yields reduced order models equipped with rigorous error bounds — is well developed for linear parametrized parabolic partial differential equations [20, 22, 26, 52]. However in the nonlinear case many open research issues remain. We shall focus in this paper on the development of rigorous *a posteriori* error bounds and rapidly and uniformly convergent reduced basis approximations for the unsteady Boussinesq equations. [a] To the extent that the unsteady Boussinesq system is a superset of the unsteady incompressible Navier–Stokes equations and (non–passive) scalar convection–diffusion equations the methods of this paper are in fact broadly applicable to many problems in fluid mechanics and transport. From a computational point of view the unsteady Navier-Stokes/Boussinesq equations are quite simple: a quadratic nonlinearity that admits

---

[a]Earlier work has established reduced basis approximations and associated rigorous *a posteriori* error bounds for nonsingular solution branches of the *steady* Burgers [55] and *steady* incompressible Navier-Stokes and Boussinesq equations [9, 14, 45, 54]; we focus here on the *unsteady* case.

standard Galerkin treatment.[b] However, from the theoretical point of view the unsteady Navier-Stokes/Boussinesq equations are very difficult [11, 36]: exponential instability seriously compromises *a priori* and *a posteriori* error estimates.

Our approach confronts but does not eliminate exponential instability in time; although in some cases [36] it may be possible to demonstrate only algebraic growth of perturbations, more generally — most simply, linearly unstable flows — we must admit exponential sensitivity to disturbances. Nevertheless, we shall demonstrate that, with careful treatment of the stability growth rate, our rigorous error bounds remain practicable for parameter domains and *finite* final times of physical and engineering interest. Equally conclusively we shall also demonstrate that rigorous error estimation remains beyond our reach for very high (say) Grashof number and large (asymptotic) final times. Note the error bounds are not only crucial for certification, but also for the efficient construction of rapidly and uniformly convergent reduced basis approximations over extended parameter domains.

Our development here is based upon our previous work on the unsteady viscous Burgers' equation [44]. Extension to incompressible Navier-Stokes equations and more generally the Boussinesq approximation introduces many new challenges: the higher spatial dimension requires greater attention to Offline cost; efficiency demands a higher order temporal discretization (here, Crank-Nicolson); the coupled momentum-energy equations for the velocity/temperature vector field require proper/balanced scaling; the incompressibility "constraint" must be accommodated in the stability eigenproblems and dual norm calculations; and greater intrinsic instability imposes additional limitations on parameter ranges and final time. Moreover, our previous work on the Burgers' equation considered only a single parameter; in the current paper we consider two parameters — Grashof number and direction of gravity (and of course time) — which places further stress on the POD-Greedy sampling procedure.

The paper is organized as follows. In Section 2 we introduce a particular natural convection problem and we formulate the unsteady Boussinesq equations in an appropriately scaled weak form. We also indicate the broader range of problems to which the methods of this paper are applicable. In Section 3 we describe our reduced basis (RB) approach for the unsteady Boussinesq equations with particular emphasis on rigorous *a posteriori* error bounds for the RB fields and associated RB outputs. In Section 4 we present numerical results illustrating RB convergence, RB error bound effectivity, and RB computational savings.

2. Problem Formulation

We now introduce a specific natural convection problem so that we may be precise in our notation and scalings and provide concrete discussion and demonstration of

---

[b]Note for higher-order and non-polynomial nonlinearities more sophisticated reduced basis approximations must be considered [6, 8, 21, 50] which in turn introduce both numerical and theoretical complications.

4   *D. J. Knezevic, N. C. Nguyen, A. T. Patera*

physical relevance. It should be emphasized, however, that our methods apply to a broad class of problems modeled by the Boussinesq superset; we discuss this further below.

2.1. *Strong Statement*

We consider flow in the two-dimensional enclosure $\tilde{\Omega} \equiv]0, 5\tilde{H}[^2 \backslash \tilde{\mathcal{P}}$, where $\tilde{\mathcal{P}}$ is the pillar (or fin) $]2.5\tilde{H} - 0.1\tilde{H}, 2.5\tilde{H} + 0.1\tilde{H}[\times]0, \tilde{H}[$; the geometry is shown in Figure 1(a).[c] The "roof" of the cavity is maintained at a constant temperature $\tilde{T}_w$, the sides and base of the cavity are perfectly thermally insulated, and the top and sides of the pillar are subjected to a uniform heat flux $\tilde{q}_w$; we impose no-slip velocity conditions on all walls. We denote the Cartesian spatial coordinate by $\tilde{x} = (\tilde{x}_1, \tilde{x}_2)$ and time by $\tilde{t}$. We further introduce the fluid properties kinematic viscosity $\tilde{\nu}$, density $\tilde{\rho}$, thermal conductivity $\tilde{k}$, thermal diffusivity $\tilde{\kappa}$, and thermal expansion coefficient $\tilde{\beta}$. Finally, the acceleration of gravity is given by $\tilde{g}(\sin\phi, \cos\phi)$.

We shall shortly introduce the governing equations for the velocity field $\tilde{V} = (\tilde{V}_1, \tilde{V}_2)$, pressure $\tilde{P}$, and temperature $\tilde{T}$. We first define the dimensionless variables $x = \frac{\tilde{x}}{\tilde{H}}$, $t = \frac{\tilde{t}\tilde{\nu}}{\tilde{H}^2}$, $V = \sqrt{\text{Ra}}\frac{\tilde{V}\tilde{H}}{\tilde{\nu}}$, $P = \frac{\tilde{P}\tilde{H}^2}{\tilde{\rho}\tilde{\nu}^2}$, $T = \text{Gr}\frac{\tilde{k}(\tilde{T}-\tilde{T}_w)}{\tilde{q}_w\tilde{H}}$ for length, time, velocity, pressure, and temperature, respectively; here the (flux-based) Grashof number Gr is given by $\text{Gr} = \tilde{g}\tilde{\beta}\tilde{q}_w\tilde{H}^4/\tilde{k}\tilde{\nu}^2$, where we recall that $\tilde{g}$ is the magnitude of the acceleration of gravity. We shall set the Prandtl number $\text{Pr} = \tilde{\nu}/\tilde{\kappa}$ to 0.71 (air). Finally, we introduce the Rayleigh number Ra given by $\text{Ra} = \text{Gr} \times \text{Pr}$.

The Boussinesq equations for the non-dimensional velocity $V(x, t)$, temperature $T(x, t)$, and pressure $P(x, t)$ are given by

$$\frac{\partial V_1}{\partial t} + \frac{1}{2\sqrt{\text{GrPr}}}\left(V_j\frac{\partial V_1}{\partial x_j} + \frac{\partial V_1 V_j}{\partial x_j}\right) + \sqrt{\text{GrPr}}\frac{\partial P}{\partial x_1} - \frac{\partial^2 V_1}{\partial x_j \partial x_j} - \sqrt{\text{GrPr}}T\sin\phi = 0,$$

$$\frac{\partial V_2}{\partial t} + \frac{1}{2\sqrt{\text{GrPr}}}\left(V_j\frac{\partial V_2}{\partial x_j} + \frac{\partial V_2 V_j}{\partial x_j}\right) + \sqrt{\text{GrPr}}\frac{\partial P}{\partial x_2} - \frac{\partial^2 V_2}{\partial x_j \partial x_j} - \sqrt{\text{GrPr}}T\cos\phi = 0,$$

$$\frac{\partial T}{\partial t} + \frac{1}{2\sqrt{\text{GrPr}}}\left(V_j\frac{\partial T}{\partial x_j} + \frac{\partial V_j T}{\partial x_j}\right) - \frac{1}{\text{Pr}}\frac{\partial^2 T}{\partial x_j \partial x_j} = 0, \quad \text{and} \quad \frac{\partial V_j}{\partial x_j} = 0,$$

corresponding to momentum, energy, and continuity. The equations are satisfied for $t \in I \equiv (0, t_f]$ where t_f is the final time, and over Ω, the non-dimensional domain shown in Figure 1(b). (Note that repeated indices imply summation.) We impose quiescent initial conditions: $V(x, 0) = 0$ and $T(x, 0) = 0$. Note that we choose the particular "balanced" scaling of variables and equations — one of many possible classical options for distributing the parameters — in order to obtain better *a posteriori* error estimates for the subsequent reduced basis approximation. Also, we choose skew-symmetric convection operators in our formulation to ensure certain discrete stability properties.

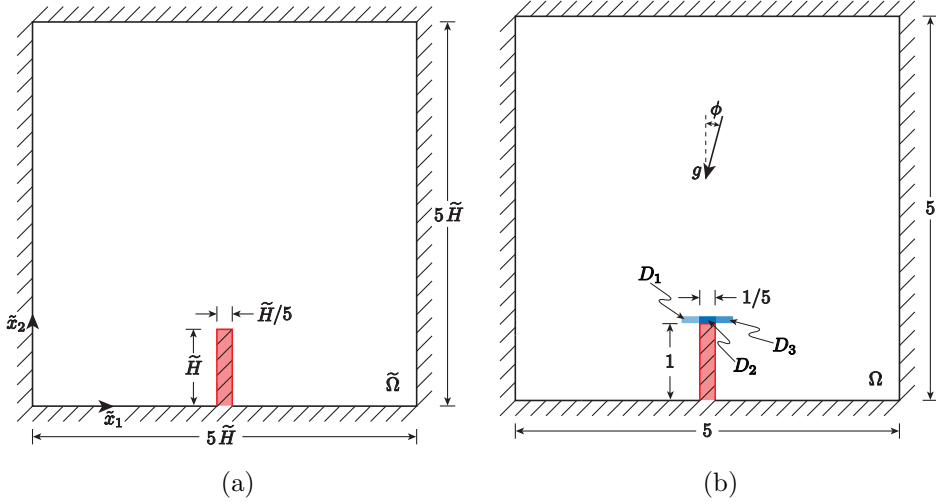[c]Note that ˜ denotes a *dimensional* quantity.

Fig. 1. (a) The computational domain in dimensional form; note that $\tilde{\Omega}$ does not include the pillar (shaded in red). (b) The dimensionless computational domain, the "direction of gravity" parameter ϕ, and the output regions D_1, D_2, and D_3.

We denote the boundary of Ω by $\partial\Omega$ and the boundary of the pillar by $\partial\mathcal{P}$ (hence $\partial\mathcal{P} \subset \partial\Omega$). We impose no-slip boundary conditions $V_1 = V_2 = 0$ on $\partial\Omega$, zero temperature, $T = 0$, on the cavity "roof" $[0,5] \times \{5\}$, zero heat flux, $\partial T/\partial n = 0$, on the sides and base of the enclosure $\partial\Omega \setminus (\partial\mathcal{P} \cup [0,5] \times \{5\})$, and inhomogeneous Neumann boundary conditions, $\partial T/\partial n = \text{Gr}$, on the pillar $\partial\mathcal{P}$. Here n denotes the unit outward normal. Note that Gr in the Neumann boundary condition appears due to our particular scaling for the temperature.

We introduce a two-tuple parameter $\mu \equiv (\mu_1, \mu_2) \equiv (\text{Gr}, \phi)$ in a prescribed (bounded) parameter domain $\mu \in \mathcal{D}$. Our goal is to study parametric dependence of the temperature in regions at or near the top of the heated pillar in the presence of natural convection. As such, our particular interest is not in the solution field *per se*, but rather in local average-temperature "outputs of interest" s_n, $n = 1, 2, 3$. These outputs can be expressed as functionals of T, namely,

$$s_n(t; \mu) = \frac{1}{\mu_1 |D_n|} \int_{D_n} T(t; \mu) \; ;$$

here $D_1 = [2.2, 2.4] \times [1, 1.1]$, $D_2 = [2.4, 2.6] \times [1, 1.1]$, and $D_3 = [2.6, 2.8] \times [1, 1.1]$ — three small rectangles above the pillar — are the subdomains over which the temperature is averaged. These output regions are depicted in Figure 1(b). Note that when we refer to a generic output (say, for numerical treatment) we shall often suppress the subscript n in s_n.

6   *D. J. Knezevic, N. C. Nguyen, A. T. Patera*

2.2. *Weak Statement and Truth Formulation*

We now introduce several notations required for the remainder of this paper. We first define the function spaces $Q \equiv \{q \in L^2(\Omega) \mid \int_\Omega q = 0\}$, $Y \equiv \{v \in (H^1(\Omega))^2 \mid v|_{\partial\Omega} = 0\}$, and $W \equiv \{w \in H^1(\Omega) \mid w = 0 \text{ on } [0,5] \times \{5\}\}$; here $H^1(\Omega) = \{v | v \in L^2(\Omega), \nabla v \in (L^2(\Omega))^2\}$, and $L^2(\Omega)$ is the space of square integrable functions over Ω. The velocity, pressure, and temperature fields will belong to Y, Q, and W, respectively. Since we shall work with incompressible velocity fields, we further introduce Z as the space of all *divergence-free* functions V in Y.

We then define $X \equiv Z \times W$; note that for any member w of X the first two components w_1 and w_2 refer to the x_1 and x_2 components of the velocity, respectively, while the third component w_3 refers to temperature. We next associate to X the inner product $(w,v)_X = \int_\Omega \frac{\partial w_i}{\partial x_j} \frac{\partial v_i}{\partial x_j}$ and induced norm $\| \cdot \|_X = \sqrt{(\cdot,\cdot)_X}$ for $w = (w_1,w_2,w_3) \in X$ and $v = (v_1,v_2,v_3) \in X$. We also define, for any members $w \in X$, $v \in X$, the $(L^2(\Omega))^3$ inner product $(w,v) = \int_\Omega w_i v_i$ and induced norm $\| \cdot \| = \sqrt{(\cdot,\cdot)}$.

We can now state the parametrized weak formulation of the governing Boussinesq equations: for given μ in the parameter domain $\mathcal{D}$ and all times $t \in I$, the velocity-temperature field $u(t;\mu) \equiv (V_1(t;\mu), V_2(t;\mu), T(t;\mu)) \in X$ satisfies

$$(u_t(t;\mu), v) + a(u(t;\mu), v; \mu) + b(u(t;\mu), v; \mu)$$
$$+ c(u(t;\mu), u(t;\mu), v; \mu) = f(v; \mu), \quad \forall\, v \in X , \quad (2.1)$$

subject to initial condition $u(t = 0; \mu) = 0$. Note that the pressure is eliminated thanks to our divergence-free velocity (test) space. We subsequently evaluate our outputs of interest as

$$s_n(t;\mu) = \ell_n(u(t;\mu); \mu), \ n = 1, 2, 3,$$

corresponding to the averaged temperatures over D_1, D_2 and D_3.

Here our forms are given by

$$a(w,v;\mu) = \int_\Omega \left(\frac{\partial w_1}{\partial x_j} \frac{\partial v_1}{\partial x_j} + \frac{\partial w_2}{\partial x_j} \frac{\partial v_2}{\partial x_j} + \frac{1}{\Pr} \frac{\partial w_3}{\partial x_j} \frac{\partial v_3}{\partial x_j} \right),$$

$$b(w,v;\mu) = -\sqrt{\mu_1 \Pr} \sin\mu_2 \int_\Omega w_3 v_1 - \sqrt{\mu_1 \Pr} \cos\mu_2 \int_\Omega w_3 v_2,$$

$$c(w,z,v;\mu) = \frac{1}{2\sqrt{\mu_1 \Pr}} \int_\Omega \left(\frac{\partial w_i z_j}{\partial x_j} + z_j \frac{\partial w_i}{\partial x_j} \right) v_i, \qquad (2.2)$$

$$f(v;\mu) = \frac{\mu_1}{\Pr} \int_{\partial\mathcal{P}} v_3,$$

$$\ell_n(v;\mu) = \frac{1}{\mu_1 |D_n|} \int_{D_n} v_3,$$

for $w = (w_1,w_2,w_3) \in X$, $v = (v_1,v_2,v_3) \in X$, and $z = (z_1,z_2,z_3) \in X$; note that in the above expressions $i = 1,2,3$ and $j = 1,2$. Recall that $\mu_1 = \mathrm{Gr}$ and $\mu_2 = \phi$.

Note that since $\ell(\cdot;\mu) \in (L^2(\Omega))^3$ and $u(\cdot;\mu) \in C^0((0,t_f);(L^2(\Omega))^3)$ [51], $s(t;\mu)$ is indeed well-defined for all $t \in I$.

We next introduce a regular triangulation of Ω, $\mathcal{T}_\Omega$. We then denote by $Y^{\mathcal{J}} \times Q^{\mathcal{J}} \subset Y \times Q$ the standard conforming $\mathbb{P}_2 - \mathbb{P}_1$ (quadratic/linear) velocity-pressure Taylor-Hood finite element approximation subspace over $\mathcal{T}_\Omega$, and by $W^{\mathcal{J}}$ the standard conforming $\mathbb{P}_2$ temperature finite element approximation subspace over $\mathcal{T}_\Omega$; we denote by $\mathcal{J}$ the dimension of $Y^{\mathcal{J}} \times Q^{\mathcal{J}} \times W^{\mathcal{J}}$. Finally, we define $Z^{\mathcal{N}} \equiv \{v \in Y^{\mathcal{J}} \mid \int_\Omega q\nabla \cdot v = 0, \forall q \in Q^{\mathcal{J}}\}$ and thus $X^{\mathcal{N}} = Z^{\mathcal{N}} \times W^{\mathcal{J}}$; we denote by $\mathcal{N}$ the dimension of $X^{\mathcal{N}}$.

We can now define the "truth" Crank-Nicolson finite element approximation. We first divide the time interval $[0,t_f]$ into K subintervals of equal length $\Delta t = t_f/K$; we then define $t^k \equiv k\Delta t$, $0 \le k \le K$. Then, given $\mu \in \mathcal{D}$, we seek $u^{\mathcal{N}\,k}(\mu) \in X^{\mathcal{N}}, 0 \le k \le K$, such that

$$
\frac{1}{\Delta t}(u^{\mathcal{N}\,k}(\mu) - u^{\mathcal{N}\,k-1}(\mu),v) + a\left(u^{\mathcal{N}\,k-1/2}(\mu),v;\mu\right) + b\left(u^{\mathcal{N}\,k-1/2}(\mu),v;\mu\right)
$$
$$
+ c\left(u^{\mathcal{N}\,k-1/2}(\mu),u^{\mathcal{N}\,k-1/2}(\mu),v;\mu\right) = f(v;\mu), \quad \forall v \in X^{\mathcal{N}}, 1 \le k \le K, \quad (2.3)
$$

subject to initial condition $u^{\mathcal{N}\,0}(\mu) = 0$; note that $u^{\mathcal{N}\,k}(\mu)$ denotes $u^{\mathcal{N}}(t^k;\mu)$ and $u^{\mathcal{N}\,k-1/2}(\mu)$ denotes $(u^{\mathcal{N}\,k-1}(\mu) + u^{\mathcal{N}\,k}(\mu))/2$. We then evaluate the outputs of interest: for $0 \le k \le K$,

$$
s_n^{\mathcal{N}\,k}(\mu) = \ell_n(u^{\mathcal{N}\,k}(\mu);\mu), \; n = 1,2,3, \tag{2.4}
$$

where $s_n^{\mathcal{N}\,k}(\mu) \equiv s_n^{\mathcal{N}}(t^k;\mu)$.

We shall build our RB approximation upon the "truth" discretization (2.3), and we shall measure the error in our RB prediction relative to $u^{\mathcal{N}\,k}(\mu) \equiv u^{\mathcal{N}}(t^k;\mu)$ and $s^{\mathcal{N}\,k}(\mu) \equiv s^{\mathcal{N}}(t^k;\mu)$. As we shall observe, the Online cost of the reduced basis evaluations shall be independent of ($\mathcal{N}$ and) $\mathcal{J}$ and furthermore our RB formulation is stable as ($\mathcal{N}$ and) $\mathcal{J} \to \infty$: we may thus choose $\mathcal{J}$ conservatively.

We pause here to consider the more general class of fluid mechanics and transport problems that may be directly treated by the particular methods presented in this paper. First, an anti–generalization: we may of course consider just the incompressible Navier–Stokes equations [28] or the incompressible Navier–Stokes equations plus "forced" convection (absent buoyancy effects). Note furthermore that the fluid and solid domains need not coincide, and hence our formulation can readily address conjugate heat transfer problems. Second, we may consider both two–dimensional and three–dimensional problems, and in fact the RB advantage is typically larger in three space dimensions [41].

Third, we may admit general boundary conditions on the temperature field but we may consider only no–slip or periodic boundary conditions — *not* outflow conditions — on the velocity. These restrictions on the velocity boundary conditions, in conjunction with the skew–symmetric treatment of the convection terms, ensures $c(z,z,z) = 0, \forall z \in X^{\mathcal{N}}$; the latter is crucial in the development of our error

bounds. Fourth, we many consider general source functions and general $(L^2(\Omega))^3$ outputs functionals for the velocity and temperature, however we can not recover the pressure — and hence we can not treat pressure outputs — due to our div–free formulation. The latter also effectively precludes the incorporation of geometric parameters.

Fifth, and finally, we can of course treat additional (non–geometric) parameters — for example, Pr in the fluid, or heterogeneous–material conductivities in a solid — so long as the affine hypothesis is honored.

3. Certified Reduced Basis Approach

3.1. *Reduced Basis Approximation*

We now turn to the reduced basis (RB) approximation [1, 18, 46–48]. The point of departure for the approach is the set of hierarchical RB approximation subspaces

$$X_N \equiv \operatorname{span} \{\xi_n, 1 \le n \le N\}, \quad 1 \le N \le N_{\max}, \tag{3.1}$$

where $\xi_n \in X^{\mathcal{N}}, 1 \le n \le N_{\max}$, is a set of mutually $(\cdot, \cdot)_X$-orthonormal basis functions. In actual practice (see Section 3.4), the spaces X_N will be generated by a POD-Greedy sampling procedure which combines spatial snapshots in time and parameter — $u^{\mathcal{N}\,k}(\mu)$ — in an optimal fashion; for our present purposes, however, X_N can in fact represent any sequence of (low-dimensional) hierarchical approximation spaces [53]. We require that $X_N \subset X^{\mathcal{N}}$, and we may hence pursue Galerkin projection with respect to (2.3).

Given $\mu \in \mathcal{D}$, we look for $u_N^k(\mu) \in X_N, 0 \le k \le K$, such that

$$\frac{1}{\Delta t}(u_N^k(\mu) - u_N^{k-1}(\mu), v) + a\left(u_N^{k-1/2}(\mu), v; \mu\right) + b\left(u_N^{k-1/2}(\mu), v; \mu\right)$$
$$+ c\left(u_N^{k-1/2}(\mu), u_N^{k-1/2}(\mu), v; \mu\right) = f(v; \mu), \quad \forall v \in X_N, 1 \le k \le K, \tag{3.2}$$

subject to initial condition $u_N^0(\mu) = 0$. We then evaluate the associated RB outputs: for $0 \le k \le K$,

$$s_{N,n}^k(\mu) = \ell_n(u_N^k(\mu); \mu), \quad n = 1, 2, 3. \tag{3.3}$$

Here $u_N^k(\mu)$ denotes $u_N(t^k; \mu)$, $u_N^{k-1/2}(\mu)$ denotes $(u_N^{k-1}(\mu) + u_N^k(\mu))/2$, and $s_{N,n}^k(\mu)$ denotes $s_{N,n}(t^k; \mu)$.

The goal of the RB approximation is simple: dimension reduction — $N \ll \mathcal{N}$ — and associated computational economies for given certified accuracy. (Online) RB evaluation is typically several orders of magnitude less expensive than the classical finite element approach [49, 53].

3.2. A posteriori *Error Estimation*

3.2.1. *The $(L^2(\Omega))^3$ Error Bound*

Rigorous, sharp, and inexpensive *a posteriori* error bounds are crucial to the general area of model reduction. We aim to develop an *a posteriori* error bound $\Delta_N^k(\mu) \equiv$

$\Delta_N(t^k; \mu), 1 \leq k \leq K$, for the L^2 error in the RB approximation such that

$$\|u^{\mathcal{N} k}(\mu) - u_N^k(\mu)\| \leq \Delta_N^k(\mu), \quad 1 \leq k \leq K, \quad \forall \mu \in \mathcal{D}, \tag{3.4}$$

for any $N = 1, \ldots, N_{\max}$.

To construct the *a posteriori* RB error bound, we need two ingredients. The first ingredient is the dual norm of the residual

$$\varepsilon_N(t^k; \mu) = \sup_{v \in X^{\mathcal{N}}} \frac{r_N(v; t^k; \mu)}{\|v\|_X}, \quad 1 \leq k \leq K, \tag{3.5}$$

where $r_N(v; t^k; \mu) \in (X^{\mathcal{N}})'$ is the residual associated with the reduced basis approximation (3.2): for $1 \leq k \leq K$,

$$r_N(v; t^k; \mu) \equiv f(v; \mu) - \frac{1}{\Delta t}\left(u_N^k(\mu) - u_N^{k-1}(\mu), v\right) - a\left(u_N^{k-1/2}(\mu), v; \mu\right)$$
$$- b\left(u_N^{k-1/2}(\mu), v; \mu\right) - c\left(u_N^{k-1/2}(\mu), u_N^{k-1/2}(\mu), v; \mu\right), \quad \forall v \in X^{\mathcal{N}}. \tag{3.6}$$

Note the dual norm is defined over $X^{\mathcal{N}}$, and not X. It is clear from standard duality arguments that

$$\varepsilon_N^2(t^k; \mu) = (\hat{e}_N(t^k; \mu), \hat{e}_N(t^k; \mu))_X, \tag{3.7}$$

where $\hat{e}_N(t^k; \mu) \in X^{\mathcal{N}}$ satisfies

$$(\hat{e}_N(t^k; \mu), v)_X = r_N(v; t^k; \mu), \quad \forall v \in X^{\mathcal{N}}, 1 \leq k \leq K; \tag{3.8}$$

$\hat{e}_N(t^k; \mu)$ is the Riesz representation for the linear functional $r_N(\cdot; t^k; \mu)$.

The second ingredient is a lower bound and upper bound,

$$\begin{array}{l} \rho_N^{\mathrm{LB}}(t^k; \mu) \leq \rho_N(t^k; \mu) \\ \rho_N^{\mathrm{UB}}(t^k; \mu) \geq \rho_N(t^k; \mu) \end{array}, \quad 1 \leq k \leq K, \quad \forall \mu \in \mathcal{D}, \tag{3.9}$$

respectively, for the stability constant $\rho_N(t^k; \mu)$ defined as

$$\rho_N(t^k; \mu) = \inf_{v \in X^{\mathcal{N}}} \frac{2c\left(u_N^{k-1/2}(\mu), v, v\right) + 2b(v, v; \mu) + a(v, v; \mu)}{\|v\|^2}. \tag{3.10}$$

The stability constant (3.10) is closely related to the absolute (monotonic decay) criterion of hydrodynamic stability theory [15, 37]. We demonstrate in [44] for the Burgers' equation in one spatial dimension that $\rho_N(t^k; \mu)$ is bounded from below; an analogous result can be proven in the present context [43]. We note that for our "proper scaling" $u_N^{k-1/2}(\mu) \approx O(\mathrm{Ra})$ and hence the c and b terms in the numerator of ρ_N are of the same order of magnitude; this balance moderates the magnitude of the stability constant.

We can now define our error bound $\Delta_N^k(\mu), 1 \leq k \leq K$, in terms of the dual norm of the residual and the lower bound for the stability constant. We first let $\tau_N^{\mathrm{LB}}(t^k; \mu) = \min(0.5\rho_N^{\mathrm{LB}}(t^k; \mu), 0), 1 \leq k \leq K$, and $\Delta t_N^*(\mu) =$

10   *D. J. Knezevic, N. C. Nguyen, A. T. Patera*

$\min(1/|\min_{1 \leq k \leq K} \tau_N^{\mathrm{LB}}(t^k; \mu)|, 1)$. Then, for $\Delta t < \Delta t_N^*(\mu)$, the *a posteriori* error bound

$$\Delta_N^k(\mu) = \sqrt{\frac{\Delta t \sum_{\ell=1}^{k} \left(\left(1 - \Delta t\, \tau_N^{\mathrm{LB}}(t^\ell; \mu)\right)^{-1} \varepsilon_N^2(t^\ell; \mu) \prod_{j=1}^{\ell-1} \frac{\left(1 + \Delta t\, \tau_N^{\mathrm{LB}}(t^j; \mu)\right)}{\left(1 - \Delta t\, \tau_N^{\mathrm{LB}}(t^j; \mu)\right)} \right)}{\prod_{\ell=1}^{k} \frac{\left(1 + \Delta t\, \tau_N^{\mathrm{LB}}(t^\ell; \mu)\right)}{\left(1 - \Delta t\, \tau_N^{\mathrm{LB}}(t^\ell; \mu)\right)}}},$$
(3.11)

satisfies (3.4) for $1 \leq k \leq K$. Since we work within a discretely divergence-free space, and furthermore insist upon a skew-symmetric convection formulation, the proof of this error bound is analogous to the Burgers case [44] — though extended here to the Crank-Nicolson temporal scheme; see Appendix B for details. Note (3.11) is simply the Crank-Nicolson version of the standard continuous-time exponential result.

For Gr sufficiently small (effective Reynolds number, $\mathrm{Re} \equiv \sqrt{\mathrm{Ra}}$, sufficiently small), $\rho_N(t^k; \mu)$ will be uniformly positive and hence error growth will be controlled; in this case, we can consider rather large times. However, for moderate Gr, $\rho_N(t^k; \mu)$ will be negative and hence our error bound will grow exponentially in time; in this case, our choice of t_f is restricted. Nevertheless, we believe our estimate (3.9),(3.10) will permit practical and rigorous error estimation for Re or Gr and t_f at which interesting nonlinear behavior occurs. There are two reasons for our optimism (in addition to the numerical results reported in a later section): (3.10) includes a viscous ($H^1(\Omega)$) stabilizing term which will somewhat constrain the minimizer and hence moderate the minimum — a candidate field large only in a thin destabilizing layer will also incur significant dissipation; $\rho_N(t; \mu)$ of (3.10) shall be estimated (conservatively but) relatively precisely — our bounds $\rho_N^{\mathrm{LB}}(t; \mu)$ and $\rho_N^{\mathrm{UB}}(t; \mu)$ of (3.9) shall reflect the full temporal and spatial structure of the RB velocity field. We discuss the bounds in greater detail in the next subsection.

3.2.2. *Output Error Bounds*

Finally, we introduce the error bounds for our outputs $s_{N,n}^k(\mu)$, $1 \leq k \leq K$, $n = 1, 2, 3$, as

$$\Delta_{N,n}^{s\,k}(\mu) \equiv \Delta_{N,n}^s(t^k; \mu) = \left(\sup_{v \in X^{\mathcal{N}}} \frac{\ell_n(v; \mu)}{\|v\|} \right) \Delta_N^k(\mu), \quad 1 \leq k \leq K, \ \ n = 1, 2, 3.$$
(3.12)

Given that $\ell_n(\cdot; \mu) \in (L^2(\Omega))^3$, it is readily demonstrated that, for $\mu \in \mathcal{D}$ and $0 < \Delta t < \Delta t_N^*(\mu)$,

$$|s_n^{\mathcal{N}\,k}(\mu) - s_{N,n}^k(\mu)| \leq \Delta_{N,n}^{s\,k}(\mu), \quad 1 \leq k \leq K, \ \ n = 1, 2, 3,$$

for any $N \in \{1, \ldots, N_{\max}\}$.

3.3. *Construction-Evaluation Decomposition*

The calculation of a reduced basis output $s_N(t^k; \mu)$ and associated output error bound $\Delta_N^s(t^k; \mu)$ admits a Construction-Evaluation decomposition. The Construction stage, performed once, is very expensive — $\mathcal{N}$-dependent; the Evaluation stage, performed many times for each new desired $\mu \in \mathcal{D}$, is very inexpensive — $\mathcal{N}$-independent. Note the reduced basis approach is particularly relevant in the real-time context and the many-query context; for the former the relevant metric is marginal cost — the (inexpensive) Evaluation stage — while for the latter the relevant metric is asymptotic average cost — again, the (inexpensive) Evaluation stage.

Since we work in discretely divergence-free subspaces, most of the details of the Construction-Evaluation decomposition can be directly imported from the Burgers case. The primary difference is that the evaluation of $\hat{e}_N \in X^{\mathcal{N}}$ in (3.8) and the calculation of the inf over $X^{\mathcal{N}}$ in (3.10) must now honor the divergence-free constraint: the Poisson problems in the Burgers case correspond to Stokes problems in the Boussinesq case. Our main intention here is to recall the operation counts for the Construction and Evaluation stages; we refer the reader to the discussion in [44] for further details. Note that in this section we presume that the ξ_n, $1 \le n \le N_{\max}$, are known; identification of the RB space is discussed in Section 3.4.

All aspects of the Construction-Evaluation decomposition rely on the affine dependence on μ of the operators. Specifically, we observe that we can write the forms given in (2.2) as

$$
\begin{aligned}
a(w, v; \mu) &= \Theta_a^1(\mu) a^1(w, v), \\
b(w, v; \mu) &= \Theta_b^1(\mu) b^1(w, v) + \Theta_b^2(\mu) b^2(w, v), \\
c(w, z, v; \mu) &= \Theta_c^1(\mu) c^1(w, z, v), \\
f(v; \mu) &= \Theta_f^1(\mu) f^1(v), \\
\ell_n(v; \mu) &= \Theta_\ell^1(\mu) \ell_n^1(v), \quad n = 1, 2, 3
\end{aligned}
\tag{3.13}
$$

where

$$
\begin{aligned}
\Theta_a^1(\mu) &= 1, & a^1(w, v) &= \int_\Omega \frac{\partial w_1}{\partial x_j}\frac{\partial v_1}{\partial x_j} + \frac{\partial w_2}{\partial x_j}\frac{\partial v_2}{\partial x_j} + \frac{1}{\Pr}\frac{\partial w_3}{\partial x_j}\frac{\partial v_3}{\partial x_j}, \\
\Theta_b^1(\mu) &= -\sqrt{\mu_1 \Pr}\sin\mu_2, & b^1(w, v) &= \int_\Omega w_3 v_1, \\
\Theta_b^2(\mu) &= -\sqrt{\mu_1 \Pr}\cos\mu_2, & b^2(w, v) &= \int_\Omega w_3 v_2, \\
\Theta_c^1(\mu) &= \frac{1}{\sqrt{\mu_1 \Pr}}, & c^1(w, z, v) &= \frac{1}{2}\int_\Omega \left(\frac{\partial w_i z_j}{\partial x_j} + z_j \frac{\partial w_i}{\partial x_j}\right) v_i, \\
\Theta_f^1(\mu) &= \frac{\mu_1}{\Pr}, & f^1(v) &= \int_{\partial \mathcal{P}} v_3, \\
\Theta_\ell^1(\mu) &= \frac{1}{\mu_1}, & \ell_n^1(v; \mu) &= \frac{1}{|D_n|}\int_{D_n} v_3.
\end{aligned}
$$

It is important to note that $\Theta_{a,b,c,f,\ell}$ are *parameter-dependent*, while a^1, b^1, b^2, c^1, f^1, and ℓ_n^1 are *parameter-independent*. We first provide a very brief discussion of

12   *D. J. Knezevic, N. C. Nguyen, A. T. Patera*

the Construction-Evaluation decomposition for the reduced basis approximation; we then consider the stability factor and reduced basis error bound.

RB approximation. In the *Construction* stage we form and store the reduced basis "mass" and "stiffness" matrices and load and output vectors associated with the time-independent and parameter-independent forms in (3.13). The operation count in the Construction stage of course depends on $\mathcal{N}$: each entry of these arrays corresponds to a quadrature over the triangulation $\mathcal{T}_\Omega$. In the *Evaluation* stage, for each Newton iteration at each time level $k = 1, \ldots, K$, we first combine the $\Theta_{a,b,c,f,\ell}(\mu)$ with the stored parameter-independent RB matrices and vectors to form the $N \times N$ RB linear system — in $O(N^3)$ operations; we then solve this RB linear system — again in $O(N^3)$ operations (in general, we must anticipate that the reduced basis matrices will be dense). Once the RB field is obtained — $O(n_{\mathrm{Newton}} N^3 K)$ operations in total, where n_{Newton} is the average number of Newton iterations per time step — we can evaluate our RB output in $O(NK)$ operations. The storage and operation count in the Evaluation stage is clearly independent of $\mathcal{N}$, and we can thus anticipate — presuming $N \ll \mathcal{N}$ — very rapid reduced basis response in the real-time and many-query contexts.

Stability Factor. We invoke (3.13) to express $\rho_N(t^k; \mu)$ of (3.10) as

$$\rho_N(t^k; \mu) = \min_{v \in X^{\mathcal{N}}} \sum_{n=1}^{N+3} \Upsilon^n(t^k; \mu) \frac{d^n(v,v)}{\|v\|^2} . \tag{3.14}$$

Here $\Upsilon^n(t^k; \mu) = \Theta_c^1(\mu)(\omega_{N\,n}^k(\mu) + \omega_{N\,n}^{k-1}(\mu))/2$, $1 \le n \le N$, $\Upsilon^{N+1}(t^k; \mu) = \Theta_b^1(\mu)$, $\Upsilon^{N+2}(t^k; \mu) = \Theta_b^2(\mu)$, and $\Upsilon^{N+3}(t^k; \mu) = \Theta_a^1(\mu)$ are *parameter-dependent* functions; correspondingly $d^n(w,v) = c(\xi_n, w, v) + c(\xi_n, v, w)$,[d] $1 \le n \le N$, $d^{N+1}(w,v) = b^1(w,v) + b^1(v,w)$, $d^{N+2}(w,v) = b^2(w,v) + b^2(v,w)$, and $d^{N+3}(w,v) = a^1(w,v)$ are *parameter-independent* bilinear forms. We then apply the Successive Constraint Method (SCM) [29,53] to implement a Construction-Evaluation decomposition for the lower bound $\rho_N^{\mathrm{LB}}(t^k; \mu)$ and upper bound $\rho_N^{\mathrm{UB}}(t^k; \mu)$.

The SCM is a general Construction-Evaluation procedure for the calculation of a *rigorous* lower bound and upper bound for the minimum of a Rayleigh quotient, such as (3.14), associated with a parametrically affine operator: the Offline stage requires solution of eigenproblems related to (3.14); the Online stage is a very small Linear Program (complexity independent of $\mathcal{N}$). The SCM methodology for the Burgers equation [44] carries over directly to the Boussinesq case except that the truth eigenvalue problems for (3.14) must be performed on our constrained "div-free" space. In order to effect the latter we consider generalized (indefinite) Stokes-type problems, the numerical treatment of which is described in Appendix A.

---

[d]A theoretical subtlety due to our minimal regularity assumption is that the $d^n(\cdot, \cdot)$ are not necessarily bounded as $\mathcal{N} \to \infty$. In actual practice this poses no difficulty for $\mathcal{N}$ finite and even $\mathcal{N}$ very large since the growth is modest and furthermore moderated by the coefficients Υ^n, $1 \le n \le N$, of our expansion (3.14).

RB Error Bounds. We now turn to the error bounds $\Delta_{N,n}^{s\,k}(\mu)$, $n = 1, 2, 3$. It is clear from (3.12) that these output error bounds $\Delta_{N,n}^{s\,k}(\mu)$, $n = 1, 2, 3$, can be directly evaluated in terms of the dual norm of ℓ_n^1 — which we can readily compute in the Construction stage — and the $L^2(\Omega)$ error bound, $\Delta_N^k(\mu)$; we thus focus on the $L^2(\Omega)$ error bound, $\Delta_N^k(\mu)$. It is furthermore clear from (3.11) that there are two components to the calculation of $\Delta_N^k(\mu)$: evaluation of $\rho_N^{\mathrm{LB}}(t^k; \mu)$ by the Successive Constraint Method (as discussed above), and computation of the dual norm of the residual, $\varepsilon_N(t^k; \mu)$ of (3.5); hence we now summarize the Construction-Evaluation decomposition for $\varepsilon_N(t^k; \mu)$.

The Construction-Evaluation decomposition of $\varepsilon_N(t^k; \mu)$ relies on the development of the Riesz representation $\hat{e}(t^k; \mu)$ as a sum of $(1 + 3N_{\max} + N_{\max}^2)$ terms each of which is the product of a parameter-independent function and a parameter-dependent member of $X^{\mathcal{N}}$ (a "Riesz piece"). In the *Construction* stage, we must first solve $1 + 3N_{\max} + N_{\max}^2$ Stokes problem over $Y^{\mathcal{J}} \times Q^{\mathcal{J}} \times W^{\mathcal{J}}$ to obtain the Riesz pieces and then form the associated $(1 + 3N_{\max} + N_{\max}^2)^2$ $(\cdot, \cdot)_X$ inner products — both steps are clearly expensive $\mathcal{N}$-dependent operations. In the *Evaluation* stage we perform a weighted summation of the stored inner products — $O(N^4)$ operations per time step and hence $O(N^4 K)$ operations in total. The operation count for the Evaluation stage is indeed independent of $\mathcal{N}$. However, the quartic scaling with N is obviously very unwelcome, and in actual practice except for modest N the cost to evaluate $\Delta_N(t^k; \mu)$ will dominate the cost to evaluate $s(t^k; \mu)$. We discuss palliatives at the conclusion of the paper.

3.4. *Offline Stage*

As discussed in the previous section, the Construction stage is performed Offline; the Evaluation stage is invoked Online — for each new μ of interest in the real-time or many-query contexts. However, there are several other components to the Offline stage as we now discuss.

In particular, there are two key "train" components to the Offline stage. First, we must identify a good (rapidly convergent) reduced basis space and associated basis functions $\xi_i, 1 \le i \le N_{\max}$. Our procedure in fact relies heavily on the Construction-Evaluation decomposition: we perform (inexpensive) error bound calculations over an RB train sample in $\mathcal{D}$ in order to greatly reduce the requisite number of (candidate) truth finite element calculations. Second, we must construct our SCM "constraint sample" — a pre-computed set of $\rho_N(t^k; \mu)$ — by a procedure described in [29, 53]. In fact, this process also relies on the Construction-Evaluation decomposition: we perform (inexpensive) stability factor lower and upper bound calculations over an SCM train sample in $\mathcal{D}$ in order to greatly reduce the requisite number of truth eigenproblem calculations. We now briefly elaborate upon the first component, the construction of the reduced basis space, in order to introduce terminology required in our discussion of the numerical results.

We apply the POD-Greedy procedure first proposed in [26]: we combine the

14   *D. J. Knezevic, N. C. Nguyen, A. T. Patera*

POD (Proper Orthogonal Decomposition) in t^k — to capture the causality associated with our evolution equation — with the Greedy procedure in μ [22, 53, 56] — to treat efficiently the higher dimensions and more extensive ranges of parameter variation. In short, in the mth cycle of the outer Greedy iteration, we first identify that parameter value μ_*^m in an extensive RB train sample $\Xi_{\text{train}} \subset \mathcal{D}$ at which the RB error bound (3.11) (at the final time) is *largest*; we then construct the POD for $u^{\mathcal{N}}(t^k; \mu_*^m) - \Pi_{X_N} u^{\mathcal{N}}(t^k; \mu_*^m), 1 \leq k \leq K$, where Π_{X_N} refers to the $(\cdot, \cdot)_X$ projection on the current reduced basis space X_N; finally, we append to our current RB space X_N (the first) ΔN POD modes in order to obtain $X_{N+\Delta N}$. The set of parameter values selected by the Greedy algorithm shall be denoted $S^* = \{\mu_*^1, \mu_*^2, \ldots, \mu_*^{n_{\text{Greedy}}}\}$, where $n_{\text{Greedy}} = N/\Delta N$ is the number of Greedy cycles; note that a particular parameter value can appear in S^* more than once.

We refer the reader to the papers [26, 40] for a detailed discussion of this POD-Greedy algorithm. We do, however, note here one important modification required in the present nonlinear context [44]. We can not compute $\Delta_N^k(\mu)$ in the POD-Greedy procedure since we can not yet evaluate $\rho_N(t^k; \mu)$ — the latter requires the RB space "under construction." Hence, in the POD-Greedy procedure we replace $\Delta_N^k(\mu)$ with a simpler estimator $\Delta_N^*(t^k; \mu)$ in which $\rho_N(t^k; \mu)$ is approximated by an inexpensive surrogate, ρ_N^* — typically a constant or a linear function of μ. Once the reduced basis spaces are defined we can then construct our SCM lower bound for the stability factor. If we find that the actual lower bound $\rho_N^{\text{LB}}(t^k; \mu)$ is in fact very different from, and in particular much more negative than, our nominal value ρ_N^* we may wish to return to the POD-Greedy algorithm in order to ensure a sufficiently accurate and sufficiently uniform reduced basis approximation. However, we typically choose ρ_N^* and our error tolerance conservatively and hence such a "restart" is not normally required. Note that in any event *in the Online stage* our stability factor, and hence our *a posteriori* error bound, is rigorous.

4. Numerical Results

In this section we present numerical results for the natural convection pillar problem described in Section 2. In order to illustrate our methodology, we consider two versions of the problem. In the first case, we fix $\phi = 0$ (gravity in the $-x_2$-direction) so that the Grashof number is our sole parameter; we consider $\text{Gr} \equiv \mu = \mu_1 \in \mathcal{D} \equiv [100, 6000]$ and $t_f = 0.2$. In the second (more difficult) case, we consider both $\text{Gr} \equiv \mu_1$ and $\phi \equiv \mu_2$ as parameters; we choose $\mathcal{D} \equiv [4000, 6000] \times [0, 0.2]$ and $t_f = 0.16$. In each case our final time is sufficiently large to observe a plume of hot air rising from the pillar. We will also observe non-monotonicity of our outputs in time — an obvious consequence of nonlinear natural convection.

We consider a Crank-Nicolson scheme with constant time step Δt corresponding to $K = 100$ time levels. For the truth spatial discretization we take a classical $\mathbb{P}_2 - \mathbb{P}_1$ (quadratic/linear) Taylor-Hood discretization [23] with a total of $\mathcal{J} = 10,161$ velocity, pressure, and temperature degrees of freedom. All computational

results were obtained via `rbOOmit` [41], a plugin for the open-source finite element library `libMesh` [39] which provides the extra functionality required for the certified RB method. We first present some truth discretization results to broadly illustrate the nature of this Boussinesq problem.

Figure 2(a) and 2(b) show the truth velocity and temperature for $(\mathrm{Gr}, \phi) = (6000, 0)$ at $t^k = 0.1$ and $t^k = 0.2$ — for this value of Grashof number we observe a plume of hot air rising from the pillar. In Figure 3(a), we display the finite element truth output $s_2^{\mathcal{N}}(t^k; \mu)$ (the "middle" output) as a function of t^k for $(\mathrm{Gr}, \phi) = (6000, 0)$ and $(\mathrm{Gr}, \phi) = (100, 0)$; the $\mathrm{Gr} = 100$ case corresponds closely to pure conduction and therefore is a convenient baseline for comparison. We note that the $\mathrm{Gr} = 6000$ output initially rises above the $\mathrm{Gr} = 100$ output but then at $t^k \approx 0.13$ the $\mathrm{Gr} = 6000$ output begins to decrease and ultimately descends below the $\mathrm{Gr} = 100$ output. This non–monotonicity can be explained in terms of the flowfield of Figure 2(a) and 2(b): for early times (hot) air is brought to D_2 from the (heated) base of the pillar; for later times the circulation pattern shifts upwards and now (cool) air is brought to D_2 from the (unheated) enclosure side walls.

In Figure 2(c) and 2(d) we show the truth field variables for $(\mathrm{Gr}, \phi) = (6000, 0.2)$ at $t^k = 0.1$ and $t^k = 0.2$. In this case the plume of hot air rises slightly to the right due to the off-vertical direction of gravity. In Figure 3(b) we display the "left" and "right" truth outputs — $s_1^{\mathcal{N}}(t^k; \mu)$ and $s_3^{\mathcal{N}}(t^k; \mu)$, respectively — as functions of t^k for $(\mathrm{Gr}, \phi) = (6000, 0.2)$, $(\mathrm{Gr}, \phi) = (5000, 0.1)$, and $(\mathrm{Gr}, \phi) = (4000, 0.05)$; we observe that the output maxima change in magnitude and shift in time as Gr is varied, and that the difference between the "left" and "right" outputs depends on ϕ in the anticipated way.

We shall now present reduced basis results for the two subproblems introduced above.

One-Parameter Case: $\mathcal{D} \equiv [100, 6000]$, $t_f = 0.2$. We choose a uniformly distributed sample $\Xi_{\mathrm{train}} \subset \mathcal{D}$ of size $n_{\mathrm{train}} = 20$ and pursue the POD-Greedy sampling procedure. In order to (coarsely) reflect the dependence of ρ on μ, we set ρ_N^* to be a linear function of Gr such that $\rho_N^*(100) = 0$ and $\rho_N^*(6000) = -60$. We set $\Delta N = 3$ and generate a reduced basis space with $N_{\max} = 66$. The optimal parameter sample S^* is shown in Figure 4(a). We observe that the parameter points are spread throughout $\mathcal{D}$ but that most of the POD-Greedy sample points are clustered at or near $\mu = \mathrm{Gr}_{\max}$; this clustering is due primarily to the biasing effect of our ρ_N^*, but also to the more complicated flow dynamics at higher Gr. We also present, in Figure 4(b), $\epsilon_{N,\max,\mathrm{rel}}^* \equiv \max_{\mu \in \Xi_{\mathrm{train}}} \frac{\Delta_N^*(t^K; \mu)}{\|u_N(t^K; \mu)\|}$ as a function of N. Clearly, the error indicator $\epsilon_{N,\max,\mathrm{rel}}^*$ decreases very rapidly; we shall subsequently confirm that the rigorous error bound, and hence the true error, also decreases very rapidly with N.

We now turn to the stability factor. We perform the SCM procedure to construct the lower bound for the stability factor. We show in Figure 5 the stability factor $\rho_N(t^k; \mu)$ as a function of t^k for $N = 66$ and two different values of μ; we also

present the stability factor lower bound $\rho_N^{\mathrm{LB}}(t^k;\mu)$ and corresponding upper bound $\rho_N^{\mathrm{UB}}(t^k;\mu)$. As already indicated, $\rho_N(t^k;\mu)$ reflects viscous stabilization effects as well as the detailed spatial and temporal structure of the RB velocity field. For $\mathrm{Gr} = 100$, $\rho_N(t^k;\mu)$ is small in magnitude and relatively constant in time; for $\mathrm{Gr} = 6000$, $\rho_N(t^k;\mu)$ is already much more negative at $t^k = 0$ and decreases further with increasing time t^k. The SCM lower bound is of sufficient accuracy for our purposes. The SCM upper bound (significantly less complicated and less costly than a standard RB Rayleigh-Ritz approximation) is very sharp; unfortunately, if we replace in our error bounds the less accurate $\rho_N^{\mathrm{LB}}(t^k;\mu)$ with the more accurate $\rho_N^{\mathrm{UB}}(t^k;\mu)$ we can no longer provide rigorous guarantees.

We present in Figure 6 the output error $|s_2^{\mathcal{N}}(t^k;\mu) - s_{N,2}(t^k;\mu)|$ and the error bound $\Delta_{N,2}^s(t^k;\mu)$ for this "middle" output as a function of t^k for (a) $N = 33$, and (b) $N = 66$, in each case for two different values of the Grashof number. First, we see that the RB error *and* RB error bound decrease rapidly as N increases; furthermore, thanks to the POD-Greedy sampling procedure, the error bound is roughly uniform over the parameter domain $\mathcal{D}$. Second, we observe that the (exponential growth of) the error bound is pessimistic: the residual clearly does not excite the most unstable "modes" in the actual error. Nevertheless, we obtain meaningful and rigorous (and, as we shall see shortly, inexpensive) error bounds.

We now turn to a more realistic "real-time" context. We show in Figure 7 the RB output $s_{N,2}(t^k;\mu)$ and associated output bounds $s_{N,2}^{\pm}(t^k;\mu) = s_{N,2}(t^k;\mu) \pm \Delta_{N,2}^s(t^k;\mu)$ as functions of t^k for $N = 33$ and $N = 66$ for three different parameter values. Note that $s_2^{\mathcal{N}}(t^k;\mu) \in [s_{N,2}^-(t^k;\mu), s_{N,2}^+(t^k;\mu)]$, $k = 1, \ldots, K$, for any $\mu \in \mathcal{D}$ and any $N \in \{1, \ldots, \mathcal{N}_{\max}\}$. As before, we observe good convergence and meaningful/useful error bounds. We note that $N = 33$ is insufficient to certifiably distinguish the outputs for different Grashof numbers: although the RB outputs are quite accurate, the error bounds are not sufficiently tight. However, with $N = 66$ we accurately and rigorously capture the truth output behavior shown in Figure 3. Absent error bounds we could not rigorously discriminate between the different behaviors observed at different Gr.

We further note that, even for $N = 66$, Online calculation of the RB output $s_{N,2}^k(\mu)$ (respectively, the RB output error bound $\Delta_{N,2}^{s\,k}(\mu)$), $1 \leq k \leq K$, is roughly $140\times$ faster (respectively, $50\times$ faster) than direct evaluation of the FE output $s_2^{\mathcal{N}\,k}(\mu), 1 \leq k \leq K$. More quantitatively, the (Online) RB calculation $\mu \to s_{N,2}^k(\mu), \Delta_{N,2}^{s\,k}(\mu)$, $1 \leq k \leq K$, and the truth finite element calculation $\mu \to s_2^{\mathcal{N}}(t^k;\mu)$, $1 \leq k \leq K$, require roughly 10 seconds and 350 seconds, respectively, on an AMD Opteron 248 processor. As indicated earlier, the Online time to evaluate $\Delta_N^{s,k}(\mu)$ will dominate the Online time to evaluate $s_N^k(\mu)$, especially for N large, due to the $O(N^4)$ complexity of the former compared to the $O(N^3)$ complexity of the latter. We note that for natural convection problems in three space dimensions the RB savings will be even more significant [41].

Two-Parameter Case: $\mathcal{D} \equiv [4000, 6000] \times [0, 0.2]$, $t_f = 0.16$. In this case, the

dimension reduction problem is significantly more challenging: as can be seen from Figure 2, even small changes in ϕ can lead to pronounced changes in the temperature and velocity fields.

In the POD-Greedy scheme we now choose a uniformly distributed sample Ξ_{train} of size $n_{\text{train}} = 100$. We take ρ_N^* to be a linear function of Gr only — ρ is quite insensitive to changes in ϕ hence it is unnecessary to introduce parametric dependence of ρ_N^* on ϕ — through the points $\rho_N^*(4000, \cdot) = -45$, $\rho_N^*(6000, \cdot) = -60$. We choose $\Delta N = 3$ and generate a reduced basis space with $N_{\max} = 75$ basis functions. The optimal parameter sample S^* is shown in Figure 8(a); as in Figure 4(a), the majority of sample points are at large Gr — although of course in the two-parameter case the sample points are also distributed in ϕ. The rapid convergence of $\epsilon_{N,\max,\text{rel}}^*$ for the two-parameter problem is illustrated in Figure 8(b).

We close this section by discussing the two-parameter results for the RB outputs and RB error bounds — relevant in a "real-time" context — shown in Figure 9. As in the one-parameter case, the error bounds converge rapidly with increasing N and are roughly uniform over $\mathcal{D}$. For $\mu = (6000, 0.2)$ the flow asymmetry is significant; the RB error bounds for $N = 75$ allow us to rigorously distinguish the "left" and "right" outputs. However, for $\mu = (4000, 0.05)$ the flow asymmetry is much more modest; we would need to increase N slightly beyond 75 in order to discriminate the now very similar "left" and "right" outputs. The Online computation time for the RB outputs $s_{N=75}^k(\mu)$ (respectively, the RB output error bounds $\Delta_{N=75}^{s\,k}(\mu)$), $1 \leq k \leq K$ is roughly $90\times$ faster (respectively, $30\times$ faster) than direct evaluation of the FE outputs $s^{\mathcal{N}k}(\mu), 1 \leq k \leq K$.

We do observe here the deleterious effect of the N^4 complexity associated with the Online error bound calculation. We expect that multi-parameter-domain hp RB approximations [2, 3, 17] will reduce the effective $N_{\max}$ and hence mitigate the effect of the $O(N^4)$ Online complexity of the RB error bound. This, in turn, should allow more efficient treatment of more parameters and more extensive parameter domains. Initial hp results are reported in [16].

5. Acknowledgments

References

1. B. O. Almroth, P. Stern, and F. A. Brogan. Automatic choice of global shape functions in structural analysis. *AIAA Journal*, 16:525–528, 1978.
2. D. Amsallem, J. Cortial, and C. Farhat. On-demand CFD-based aeroelastic predictions using a database of reduced-order bases and models. In *47th AIAA Aerospace Sciences Meeting*, 2009.

18 *D. J. Knezevic, N. C. Nguyen, A. T. Patera*

3. D. Amsallem and C. Farhat. Interpolation method for adapting reduced-order models and application to aeroelasticity. *AIAA Journal*, 46(7):1803–1813, 2008.

4. H. Asan. Natural convection in an anulus between two isothermal square ducts. *Int. Comm. Heat Mass Transfer*, 27(3):367–376, 2000.

5. C.G. Baker and R.B. Lehoucq. Preconditioning constrained eigenvalue problems. *Linear algebra and its applications*, 431:396–408, 2009.

6. M. Barrault, Y.Maday, N. C. Nguyen, and A. T. Patera. An "empirical interpolation" method: Application to efficient reduced-basis discretization of partial differential equations. *C. R. Acad. Sci. Paris, Série I.*, 339:667–672, 2004.

7. J. Burkardt, M. D. Gunzburger, and H. C. Lee. POD and CVT-based reduced order modeling of Navier-Stokes flows. *Comp. Meth. Applied Mech.*, 196:337–355, 2006.

8. E. Cancès, C. Le Bris, N. C. Nguyen, Y. Maday, A. T. Patera, and G. S. H. Pau. Feasibility and competitiveness of a reduced basis approach for rapid electronic structure calculations in quantum chemistry. In *Proceedings of the Workshop for High-dimensional Partial Differential Equations in Science and Engineering (Montreal)*, 2007.

9. C. Canuto, T. Tonn, and K. Urban. A posteriori error analysis of the reduced basis method for nonaffine parametrized nonlinear PDEs. *SIAM J. Numer. Anal.*, 47:2001–2022, 2009.

10. E. A. Christensen, M. Brons, and J. N. Sorensen. Evaluation of POD-based decomposition techniques applied to parameter-dependent non-turbulent flows. *SIAM J. Sci. Comput.*, 21:1419–1434, 2000.

11. P. Constantin and C. Foias. *Navier-Stokes Equations*. Chicago Lectures in Mathematics. University of Chicago Press, Chicago, IL, 1988.

12. J. H. Curry, J. R. Herring, J. Loncaric, and S. A. Orszag. Order and disorder in two- and three-dimensional Bénard convection. *Journal of Fluid Mechanics*, 147:1–38, 1984.

13. A.E. Deane, I.G. Kevrekidis, G.E. Karniadakis, and S.A. Orszag. Low-dimensional models for complex geometry flows: Application to grooved channels and circular cylinders. *Phys. Fluids*, 10:2337–2354, 1991.

14. S. Deparis. Reduced basis error bound computation of parameter-dependent Navier–Stokes equations by the natural norm approach. *SIAM Journal of Numerical Analysis*, 46:2039–2067, 2008.

15. P.G. Drazin and W.H. Reid. *Hydrodynamic Stability*. Cambridge University Press, 2004.

16. J. L. Eftang, D. J. Knezevic, A. T. Patera, and E. M. Rønquist. An *hp* certified reduced basis method for parametrized time-dependent partial differential equations. Submitted to MCMDS, 2010.

17. J.L. Eftang, A.T. Patera, and E.M. Rønquist. An "hp" certified reduced basis method for parametrized parabolic partial differential equations. 2009.

18. J. P. Fink and W. C. Rheinboldt. On the error behavior of the reduced basis technique for nonlinear finite element approximations. *Z. Angew. Math. Mech.*, 63(1):21–28, 1983.

19. A. Yu. Gelfgat, P. Z. Bar-Yoseph, and A. L. Yarin. Stability of multiple steady states of convection in laterally heated cavities. *Journal of Fluid Mechanics*, 388:315–334, 1999.

20. M. Grepl. *Reduced-Basis Approximations and* A Posteriori *Error Estimation for Parabolic Partial Differential Equations*. PhD thesis, Massachusetts Institute of Technology, May 2005.

21. M. A. Grepl, Y. Maday, N. C. Nguyen, and A. T. Patera. Efficient reduced-basis treat-

ment of nonaffine and nonlinear partial differential equations. *M2AN (Math. Model. Numer. Anal.)*, 41:575–605, 2007.

22. M. A. Grepl and A. T. Patera. *A Posteriori* error bounds for reduced-basis approximations of parametrized parabolic partial differential equations. *M2AN (Math. Model. Numer. Anal.)*, 39(1):157–181, 2005.

23. M. D. Gunzburger. *Finite Element Methods for Viscous Incompressible Flows*. Academic Press, 1989.

24. M. D. Gunzburger, J. Peterson, and J. N. Shadid. Reduced-order modeling of time-dependent PDEs with multiple parameters in the boundary data. *Comp. Meth. Applied Mech.*, 196:1030–1047, 2007.

25. M.Y. Ha, I. Kim, H.S. Yoon, K.S. Yoon, J.R. Lee, S. Balanchandar, and H.H. Chun. Two-dimensional and unsteady natural convection in a horizontal enclosure with a square body. *Numerical heat transfer, Part A: Applications*, 41(2):183–210, 2002.

26. B. Haasdonk and M. Ohlberger. Reduced basis method for finite volume approximations of parametrized evolution equations. *Mathematical Modelling and Numerical Analysis (M2AN)*, 42(2):277–302, 2008.

27. M. Hinze and S. Volkwein. Proper orthogonal decomposition surrogate models for nonlinear dynamical systems: error estimates and suboptimal control. In *Lecture Notes in Computational Science and Engineering*, volume 45. Springer, 2005.

28. D. B. P. Huynh, D. J. Knezevic, J. W. Peterson, and A. T. Patera. High-fidelity real-time simulation on deployed platforms. *submitted to Computers and Fluids*, 2010.

29. D. B. P. Huynh, G. Rozza, S. Sen, and A. T. Patera. A successive constraint linear optimization method for lower bounds of parametric coercivity and inf-sup stability constants. *C. R. Acad. Sci. Paris, Analyse Numérique*, 345(8):473–478, 2007.

30. J.M. Hyun and J.W. Lee. Numerical solutions for transient natural convection in a square cavity with different sidewall temperatures. *Int. J. Heat and Fluid Flow*, 10(2), 1989.

31. K. Ito and S. S. Ravindran. A reduced basis method for control problems governed by PDEs. In W. Desch, F. Kappel, and K. Kunisch, editors, *Control and Estimation of Distributed Parameter Systems*, pages 153–168. Birkhäuser, 1998.

32. K. Ito and S. S. Ravindran. A reduced-order method for simulation and control of fluid flows. *Journal of Computational Physics*, 143(2):403–425, 1998.

33. K. Ito and S. S. Ravindran. Reduced basis method for optimal control of unsteady viscous flows. *International Journal of Computational Fluid Dynamics*, 15(2):97–113, 2001.

34. K. Ito and J. D. Schroeter. Reduced order feedback synthesis for viscous incompressible flows. *Mathematical And Computer Modelling*, 33(1-3):173–192, 2001.

35. P. S. Johansson, H.I. Andersson, and E.M. Rønquist. Reduced-basis modeling of turbulent plane channel flow. *Computers and Fluids*, 35(2):189–207, 2006.

36. C. Johnson, R. Rannacher, and M. Boman. Numerical and hydrodynamic stability: Towards error control in computational fluid dynamics. *SIAM Journal of Numerical Analysis*, 32(4):1058–1079, 1995.

37. D.D. Joseph. *Stability of fluid motions. I. & II.*, volume 27 & 28 of *Springer Tracts in Natural Philosophy*. Springer-Verlag, New York, 1976.

38. B.S. Kim, D.S. Lee, M.Y. Ha, and H.S. Yoon. A numerical study of natural convection in a square enclosure with a circular cylinder at different vertical locations. *International Journal of Heat and Mass Transfer*, 51(7-8):1888–1906, 2008.

39. B. S. Kirk, J. W. Peterson, R. M. Stogner, and G. F. Carey. libMesh: A C++ library for parallel adaptive mesh refinement/coarsening simulations. *Engineering with Computers*, 23(3–4):237–254, 2006.

20   *D. J. Knezevic, N. C. Nguyen, A. T. Patera*

40. D. J. Knezevic and A. T. Patera. A certified reduced basis method for the Fokker–Planck equation of dilute polymeric fluids: FENE dumbbells in extensional flow. *Submitted to SIAM J. Sci. Comput., May 2009.*

41. D. J. Knezevic and J. W. Peterson. A high-performance parallel implementation of the certified reduced basis method. *Submitted to CMAME.*

42. E. Lorenz. Empirical orthogonal function and statistical weather prediction. *Rep. No. 1, Statistical Forecasting Program, Dept. of Meteorology, MIT*, 1956.

43. Y. Maday. Private communication.

44. N. C. Nguyen, G. Rozza, and A. T. Patera. Reduced basis approximation and a posteriori error estimation for the time-dependent viscous Burgers equation. *Calcolo*, 2008.

45. N. C. Nguyen, K. Veroy, and A. T. Patera. Certified real-time solution of parametrized partial differential equations. In S. Yip, editor, *Handbook of Materials Modeling*, pages 1523–1558. Springer, 2005.

46. A. K. Noor and J. M. Peters. Reduced basis technique for nonlinear analysis of structures. *AIAA Journal*, 18(4):455–462, 1980.

47. T. A. Porsching. Estimation of the error in the reduced basis method solution of nonlinear equations. *Mathematics of Computation*, 45(172):487–496, 1985.

48. T. A. Porsching and M. Y. Lin Lee. The reduced-basis method for initial value problems. *SIAM Journal of Numerical Analysis*, 24:1277–1287, 1987.

49. C. Prud'homme, D. Rovas, K. Veroy, Y. Maday, A.T. Patera, and G. Turinici. Reliable real-time solution of parametrized partial differential equations: Reduced-basis output bounds methods. *Journal of Fluids Engineering*, 124(1):70–80, 2002.

50. A. Quarteroni and G. Rozza. Numerical solution of parametrized Navier-Stokes equations by reduced basis method. *Num. Meth. PDEs*, 23:923–948, 2007.

51. A. Quarteroni and A. Valli. *Numerical Approximation of Partial Differential Equations*. Springer, 2nd edition, 1997.

52. D. Rovas, L. Machiels, and Y. Maday. Reduced basis output bounds methods for parabolic problems. *IMA J. Appl. Math.*, 2005.

53. G. Rozza, D. B. P. Huynh, and A. T. Patera. Reduced basis approximation and a posteriori error estimation for affinely parametrized elliptic coercive partial differential equations: Application to transport and continuum mechanics. *Archives Computational Methods in Engineering*, 15(4), 2008.

54. K. Veroy and A. T. Patera. Certified real-time solution of the parametrized steady incompressible Navier-Stokes equations; Rigorous reduced-basis *a posteriori* error bounds. *International Journal for Numerical Methods in Fluids*, 47:773–788, 2005.

55. K. Veroy, C. Prud'homme, and A. T. Patera. Reduced-basis approximation of the viscous Burgers equation: Rigorous *a posteriori* error bounds. *C. R. Acad. Sci. Paris, Série I*, 337(9):619–624, 2003.

56. K. Veroy, C. Prud'homme, D. V. Rovas, and A. T. Patera. *A Posteriori* error bounds for reduced-basis approximation of parametrized noncoercive and nonlinear elliptic partial differential equations. In *Proceedings of the 16th AIAA Computational Fluid Dynamics Conference*, 2003. Paper 2003-3847.

57. J.L. Wright, H. Jin, K.G.T. Hollands, and D. Naylor. Flow visualization of natural convection in a tall, air-filled vertical cavity. *International Journal of Heat and Mass Transfer*, 49:889–904, 2006.

Appendix A. Stokes Eigenvalue Problem for the Stability Factor

We first note from (3.14) that the stability factor $\rho_N(t^k;\mu) = \lambda_1^{\mathcal{N}}(t^k;\mu)$, where $\lambda_1^{\mathcal{N}}(t^k;\mu)$ is the smallest eigenvalue[e] of the following generalized eigenvalue problem: given $(t^k;\mu) \in [0, t_f] \times \mathcal{D}$, find $(\chi^{\mathcal{N}}(t^k;\mu), \lambda^{\mathcal{N}}(t^k;\mu)) \in X^{\mathcal{N}} \times \mathbb{R}$ such that

$$\sum_{n=1}^{N+3} \Upsilon^n(t^k;\mu)d^n(\chi^{\mathcal{N}}, \psi) = \lambda^{\mathcal{N}}(\chi^{\mathcal{N}}, \psi), \quad \forall \psi \in X^{\mathcal{N}}, \tag{A.1}$$

and $\|\chi^{\mathcal{N}}(t^k;\mu)\| = 1$. Note that this eigenvalue problem is symmetric but (for sufficiently large Gr) indefinite. Moreover, (A.1) is a constrained problem as it is posed over the space $X^{\mathcal{N}}$.

A recent paper by Baker & Lehoucq [5] discusses general iterative strategies for solution of constrained eigenvalue problems. However, we pursue a simpler approach for this class of problem since we are only interested in $\lambda_1^{\mathcal{N}}(t^k;\mu)$. Consider the following parabolic equation on Ω

$$\left(\frac{\partial z}{\partial \tau}, \psi\right) + \sum_{n=1}^{N+3} \Upsilon^n(t;\mu)d^n(z, \psi) = 0, \qquad \forall \psi \in X^{\mathcal{N}}, \tag{A.2}$$

with $z(x, 0) = g(x)$ on Ω. It follows straightforwardly that

$$z(x, \tau) = \sum_{m=1}^{\infty} g_m \exp(-\lambda_m^{\mathcal{N}}(t^k;\mu)\,\tau)\,\chi_m^{\mathcal{N}}(x;t^k;\mu), \tag{A.3}$$

where $g_m = (g, \chi_m^{\mathcal{N}}(t^k;\mu))$. Assuming $g_1 \neq 0$, the exponential behavior in (A.3) implies that $\chi_1^{\mathcal{N}}(t^k;\mu)$ will be the dominant component of z for large t — therefore, analogously to a power method, it is possible to approximate $\lambda_1^{\mathcal{N}}(t^k;\mu)$ by a simple time-stepping approach.

The argument above is written formally in terms of the constrained space $X^{\mathcal{N}}$, where $X^{\mathcal{N}} = Z^{\mathcal{N}} \times W^{\mathcal{J}}$ and $Z^{\mathcal{N}} \equiv \{\psi \in Y^{\mathcal{J}} \mid \int_{\Omega} q\nabla \cdot \psi = 0, \forall q \in Q^{\mathcal{J}}\}$; however, in practice we impose the divergence-free constraint through a standard "pressure" Lagrange multipler. We also apply a backward Euler scheme to discretize (A.2) in time. This yields the following fully discrete parabolic Stokes-type problem

$$\begin{bmatrix} (M + \Delta\tau A(t^k;\mu)) & P \\ P^T & 0 \end{bmatrix} \begin{bmatrix} z(\tau^j) \\ p(\tau^j) \end{bmatrix} = \begin{bmatrix} M & 0 \\ 0 & 0 \end{bmatrix} \begin{bmatrix} z(\tau^{j-1}) \\ p(\tau^{j-1}) \end{bmatrix}, \tag{A.4}$$

for $j \geq 1$. Here M, A and P are the truth mass, stiffness, and gradient matrices associated with the bilinear forms

$$\sum_{n=1}^{N+3} \Upsilon^n(t^k;\mu)d^n(w, v), \;\; (w, v), \;\; \int_{\Omega} q^{\mathcal{J}} \nabla \cdot w, \tag{A.5}$$

respectively.

We then apply the restarted "pseudo-Lanczos" time-stepping algorithm given in Algorithm 1 to approximate $\lambda_1^{\mathcal{N}}(t^k;\mu)$. According to (A.3), steps 2–5 of Algorithm 1

---

[e]We adopt the convention that $\lambda_1^{\mathcal{N}}(t^k;\mu) \leq \lambda_2^{\mathcal{N}}(t^k;\mu) \leq \ldots \leq \lambda_{\mathcal{N}}^{\mathcal{N}}(t^k;\mu)$.

Algorithm 1 Pseudo-Lanczos time-stepping scheme

1: Choose $\Delta\tau$ and n_{restart}, initialize $z(\tau^0) \in X^{\mathcal{N}}$ randomly and set $\lambda^*_{\min} = \infty$;
2: **for** $j = 1, \ldots, n_{\text{restart}}$ **do**
3:     Solve (A.4) and set the jth column of $\mathbb{Z}$ to $u(\tau^j)$;
4: **end for**
5: Orthonormalize $\mathbb{Z}$ with respect to M;
6: Solve the reduced eigenvalue problem $\mathbb{Z}^T A \mathbb{Z} x_i^r = \lambda_i^r x_i^r$, $i = 1, \ldots, n_{\text{restart}}$;
7: **if** $|\lambda_1^r - \lambda^*_{\min}| < \text{TOL}$ **then**
8:     Set $\lambda_1^{\mathcal{N}}(t^k; \mu) = \lambda_1^r$, $\chi_1^{\mathcal{N}}(t^k; \mu) = \mathbb{Z} x_1^r$ and terminate;
9: **else**
10:     Set $z(\tau^0) = \mathbb{Z} x_1^r$, $\lambda^*_{\min} = \lambda_1^r$ and return to 2;
11: **end if**

---

will yield a basis — the columns of $\mathbb{Z}$ — that is strongly biased towards $\chi_1^{\mathcal{N}}(t^k; \mu)$, and hence in step 6 the minimum eigenvalue of the reduced eigenvalue problem will well approximate $\lambda_1^{\mathcal{N}}(t^k; \mu)$. We perform a restart in steps 7–11 in order to *(i)* limit τ^j and hence avoid numerical overflow issues, *(ii)* accelerate eigenvalue/eigenvector convergence, and *(iii)* limit the size of the dense reduced eigenvalue problem.

Finally, note that the choice of $\Delta\tau$ in Algorithm 1 can be important. Suppose that $z(\tau^j) = \sum_m \alpha_m^j \chi_m^{\mathcal{N}}$; then the backward Euler time-stepping scheme scales the mth coefficient as

$$\alpha_m^j = \alpha_m^{j-1}/(1 + \lambda_m^{\mathcal{N}} \Delta\tau).$$

Therefore, the mode for which $|1 + \lambda_m^{\mathcal{N}} \Delta\tau|$ is minimized will be most strongly amplified. For $\lambda_1^{\mathcal{N}} < 0$, it is possible for $1 + \lambda_1^{\mathcal{N}} \Delta\tau$ to be negative and in particular greater than unity in modulus, in which case an internal eigenmode may be amplified most strongly and we risk convergence to the wrong eigenvalue. To ensure convergence to the correct mode, $\Delta\tau$ should be chosen sufficiently small such that $|\lambda_1^{\mathcal{N}} \Delta\tau| < 1$.

Algorithm 1 has been verified by confirmation of the critical Reynolds number for the plane Poiseuille flow monotonic decay criterion [15, 37].

Appendix B. Proof of Proposition 3.1

We note from (2.3) and (3.6) that the errors $e^{\ell-1}(\mu) \equiv u^{\mathcal{N}\,\ell-1}(\mu) - u_N^{\ell-1}(\mu)$ and $e^{\ell}(\mu) \equiv u^{\mathcal{N}\,\ell}(\mu) - u_N^{\ell}(\mu)$ satisfy

$$\begin{aligned}
\frac{1}{\Delta t}\big(e^{\ell}(\mu) - e^{\ell-1}(\mu), v\big) + c\big(u^{\mathcal{N}\,\ell-1/2}(\mu), u^{\mathcal{N}\,\ell-1/2}(\mu), v; \mu\big) \\
- c\big(u_N^{\ell-1/2}(\mu), u_N^{\ell-1/2}(\mu), v; \mu\big) + a\big(e^{\ell-1/2}(\mu), v; \mu\big) \\
+ b\big(e^{\ell-1/2}(\mu), v; \mu\big) = r_N(v; t^{\ell}; \mu), \quad \forall v \in X^{\mathcal{N}}. \quad \text{(B.1)}
\end{aligned}$$

From the definition of the trilinear form c in (2.2) we can derive the following equality

$$
\begin{aligned}
c\big(u^{\mathcal{N}\,\ell-1/2}(\mu), u^{\mathcal{N}\,\ell-1/2}(\mu), v; \mu\big) &- c\big(u_N^{\ell-1/2}(\mu), u_N^{\ell-1/2}(\mu), v; \mu\big) = \\
& c\big(e^{\ell-1/2}(\mu), e^{\ell-1/2}(\mu), v; \mu\big) + c\big(u_N^{\ell-1/2}(\mu), e^{\ell-1/2}(\mu), v; \mu\big) \\
& \qquad + c\big(e^{\ell-1/2}(\mu), u_N^{\ell-1/2}(\mu), v; \mu\big), \quad \forall v \in X^{\mathcal{N}}. \quad \text{(B.2)}
\end{aligned}
$$

It thus follows from (B.1) and (B.2) and from choosing $v = e^{\ell-1/2}(\mu)$ that

$$
\begin{aligned}
\frac{1}{\Delta t}\big(e^{\ell}(\mu) &- e^{\ell-1}(\mu), e^{\ell-1/2}(\mu)\big) + c\big(e^{\ell-1/2}(\mu), e^{\ell-1/2}(\mu), e^{\ell-1/2}(\mu); \mu\big) \\
&+ c\big(u_N^{\ell-1/2}(\mu), e^{\ell-1/2}(\mu), e^{\ell-1/2}(\mu); \mu\big) + c\big(e^{\ell-1/2}(\mu), u_N^{\ell-1/2}(\mu), e^{\ell-1/2}(\mu); \mu\big) \\
&\qquad + a\big(e^{\ell-1/2}(\mu), e^{\ell-1/2}(\mu); \mu\big) + b\big(e^{\ell-1/2}(\mu), e^{\ell-1/2}(\mu); \mu\big) \\
&\qquad\qquad\qquad\qquad\qquad\qquad\qquad = r_N(e^{\ell-1/2}(\mu); t^{\ell}; \mu), \quad \text{(B.3)}
\end{aligned}
$$

which can be rewritten as

$$
\begin{aligned}
\frac{1}{\Delta t}\big(e^{\ell}(\mu) &- e^{\ell-1}(\mu), e^{\ell-1/2}(\mu)\big) + c\big(u_N^{\ell-1/2}(\mu), e^{\ell-1/2}(\mu), e^{\ell-1/2}(\mu); \mu\big) \\
&+ a\big(e^{\ell-1/2}(\mu), e^{\ell-1/2}(\mu); \mu\big) + b\big(e^{\ell-1/2}(\mu), e^{\ell-1/2}(\mu); \mu\big) = r_N(e^{\ell-1/2}(\mu); t^{\ell}; \mu),
\end{aligned}
$$
$$\text{(B.4)}$$

since

$$
\begin{aligned}
c\big(e^{\ell-1/2}(\mu), &e^{\ell-1/2}(\mu), e^{\ell-1/2}(\mu); \mu\big) \\
&= \frac{1}{2\sqrt{\mu_1 \mathrm{Pr}}} \int_{\Omega} \left(\frac{\partial e_i^{\ell-1/2} e_j^{\ell-1/2}}{\partial x_j} + e_j^{\ell-1/2} \frac{\partial e_i^{\ell-1/2}}{\partial x_j} \right) e_i^{\ell-1/2} \\
&= \frac{1}{2\sqrt{\mu_1 \mathrm{Pr}}} \int_{\Omega} \left(\frac{\partial (e_i^{\ell-1/2})^2 e_j^{\ell-1/2}}{\partial x_j} \right) \\
&= \frac{1}{2\sqrt{\mu_1 \mathrm{Pr}}} \int_{\partial\Omega} \left((e_i^{\ell-1/2})^2 e_j^{\ell-1/2} \right) n_j \\
&= 0, \quad\quad\quad\quad\quad\quad\quad\quad\quad\quad\quad\quad\quad\quad\quad\quad\quad\quad \text{(B.5)}
\end{aligned}
$$

and

$$
\begin{aligned}
c\big(e^{\ell-1/2}(\mu), &u_N^{\ell-1/2}(\mu), e^{\ell-1/2}(\mu); \mu\big) \\
&= \frac{1}{2\sqrt{\mu_1 \mathrm{Pr}}} \int_{\Omega} \left(\frac{\partial e_i^{\ell-1/2} u_{N\,j}^{\ell-1/2}}{\partial x_j} + u_{N\,j}^{\ell-1/2} \frac{\partial e_i^{\ell-1/2}}{\partial x_j} \right) e_i^{\ell-1/2} \\
&= \frac{1}{2\sqrt{\mu_1 \mathrm{Pr}}} \int_{\Omega} \left(\frac{\partial (e_i^{\ell-1/2})^2 u_{N\,j}^{\ell-1/2}}{\partial x_j} \right) \\
&= \frac{1}{2\sqrt{\mu_1 \mathrm{Pr}}} \int_{\partial\Omega} \left((e_i^{\ell-1/2})^2 u_{N\,j}^{\ell-1/2} \right) n_j \\
&= 0, \quad\quad\quad\quad\quad\quad\quad\quad\quad\quad\quad\quad\quad\quad\quad\quad\quad\quad \text{(B.6)}
\end{aligned}
$$

24 D. J. Knezevic, N. C. Nguyen, A. T. Patera

due to the non-slip boundary conditions.

The right-hand side of (B.4) can be bounded as

$$r_N(e^{\ell-1/2}(\mu); t^\ell; \mu) \leq \varepsilon_N(t^\ell; \mu)\|e^{\ell-1/2}(\mu)\|_X$$
$$\leq \frac{1}{2}\Big(\varepsilon_N^2(t^\ell; \mu) + \|e^{\ell-1/2}(\mu)\|_X^2\Big)$$
$$\leq \frac{1}{2}\Big(\varepsilon_N^2(t^\ell; \mu) + a\big(e^{\ell-1/2}(\mu), e^{\ell-1/2}(\mu); \mu\big)\Big), \quad \text{(B.7)}$$

where we use (3.5) in the first inequality, the Young's inequality, $AB \leq (A^2+B^2)/2$, in the second inequality, and (recalling that we consider $\Pr = 0.71$) $a(w, w; \mu) \geq \|w\|_X^2, \forall \mu \in \mathcal{D}$, in the third inequality. It thus follows from (B.4) and (B.7) that

$$\frac{1}{\Delta t}\big((e^\ell(\mu), e^\ell(\mu)) - (e^{\ell-1}(\mu), e^{\ell-1}(\mu))\big) + 2c\big(u_N^{\ell-1/2}(\mu), e^{\ell-1/2}(\mu), e^{\ell-1/2}(\mu); \mu\big)$$
$$+ a\big(e^{\ell-1/2}(\mu), e^{\ell-1/2}(\mu); \mu\big) + 2b\big(e^{\ell-1/2}(\mu), e^{\ell-1/2}(\mu); \mu\big) \leq \varepsilon_N^2(t^\ell; \mu). \quad \text{(B.8)}$$

Hence, from (B.8) and (3.9)-(3.10) we obtain

$$\big(e^\ell(\mu), e^\ell(\mu)\big) - \big(e^{\ell-1}(\mu), e^{\ell-1}(\mu)\big)$$
$$+ \Delta t \rho_N^{\mathrm{LB}}(t^\ell; \mu)\big(e^{\ell-1/2}(\mu), e^{\ell-1/2}(\mu)\big) \leq \Delta t \varepsilon_N^2(t^\ell; \mu).$$

We note that if $\rho_N^{\mathrm{LB}}(t^\ell; \mu) \geq 0$, then the last term on the left-hand side is non-negative and can be neglected. On the other hand, if $\rho_N^{\mathrm{LB}}(t^\ell; \mu) < 0$ we apply the Cauchy-Schwarz inequality and Young's inequality to obtain

$$\frac{1}{2}\rho_N^{\mathrm{LB}}(t^\ell; \mu)\big((e^{\ell-1}(\mu), e^{\ell-1}(\mu)) + (e^\ell(\mu), e^\ell(\mu))\big) \leq \rho_N^{\mathrm{LB}}(t^\ell; \mu)\big(e^{\ell-1/2}(\mu), e^{\ell-1/2}(\mu)\big).$$

Hence, appealing to the definition of τ_N^{LB}, we get

$$\big(e^\ell(\mu), e^\ell(\mu)\big) - \big(e^{\ell-1}(\mu), e^{\ell-1}(\mu)\big)$$
$$+ \Delta t \tau_N^{\mathrm{LB}}(t^\ell; \mu)\big((e^{\ell-1}(\mu), e^{\ell-1}(\mu)) + (e^\ell(\mu), e^\ell(\mu))\big) \leq \Delta t \varepsilon_N^2(t^\ell; \mu),$$

which after rearranging the terms yields

$$(1 + \Delta t \tau_N^{\mathrm{LB}}(t^\ell; \mu))\big(e^\ell(\mu), e^\ell(\mu)\big) - (1 - \Delta t \tau_N^{\mathrm{LB}}(t^\ell; \mu))\big(e^{\ell-1}(\mu), e^{\ell-1}(\mu)\big)$$
$$\leq \Delta t \varepsilon_N^2(t^\ell; \mu).$$

We multiply $\big(1 - \Delta t\, \tau_N^{\mathrm{LB}}(t^\ell; \mu)\big)^{-1} \prod_{j=1}^{\ell-1}\big(1 + \Delta t\, \tau_N^{\mathrm{LB}}(t^j; \mu)\big)\big(1 - \Delta t\, \tau_N^{\mathrm{LB}}(t^j; \mu)\big)^{-1}$ on both sides of the above equation to obtain

$$\big(e^\ell(\mu), e^\ell(\mu)\big) \prod_{j=1}^{\ell} \frac{\big(1 + \Delta t\, \tau_N^{\mathrm{LB}}(t^j; \mu)\big)}{\big(1 - \Delta t\, \tau_N^{\mathrm{LB}}(t^j; \mu)\big)}$$
$$- \big(e^{\ell-1}(\mu), e^{\ell-1}(\mu)\big) \prod_{j=1}^{\ell-1} \frac{\big(1 + \Delta t\, \tau_N^{\mathrm{LB}}(t^j; \mu)\big)}{\big(1 - \Delta t\, \tau_N^{\mathrm{LB}}(t^j; \mu)\big)} \leq$$
$$\Delta t\, \varepsilon_N^2(t^\ell; \mu)\big(1 - \Delta t\, \tau_N^{\mathrm{LB}}(t^\ell; \mu)\big)^{-1} \prod_{j=1}^{\ell-1} \frac{\big(1 + \Delta t\, \tau_N^{\mathrm{LB}}(t^j; \mu)\big)}{\big(1 - \Delta t\, \tau_N^{\mathrm{LB}}(t^j; \mu)\big)}. \quad \text{(B.9)}$$

Summing this equation from $\ell = 1$ to k and recalling $e(t^0; \mu) = 0$, we arrive at

$$\left(e^k(\mu), e^k(\mu)\right) \prod_{\ell=1}^k \frac{\left(1 + \Delta t\, \tau_N^{\mathrm{LB}}(t^\ell; \mu)\right)}{\left(1 - \Delta t\, \tau_N^{\mathrm{LB}}(t^\ell; \mu)\right)} \leq$$

$$\Delta t \sum_{\ell=1}^k \varepsilon_N^2(t^\ell; \mu) \prod_{j=1}^{\ell-1} \left(1 - \Delta t\, \tau_N^{\mathrm{LB}}(t^\ell; \mu)\right)^{-1} \frac{\left(1 + \Delta t\, \tau_N^{\mathrm{LB}}(t^j; \mu)\right)}{\left(1 - \Delta t\, \tau_N^{\mathrm{LB}}(t^j; \mu)\right)}, \quad \text{(B.10)}$$

for $k = 1, \dots, K$. This gives the desired result.
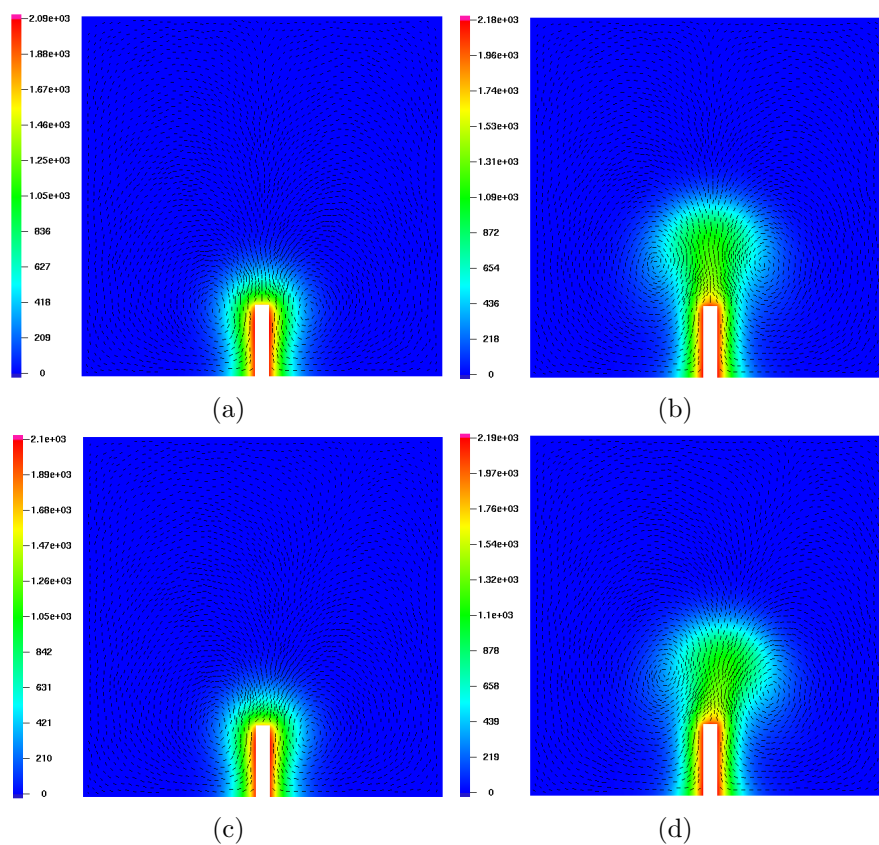
Fig. 2. The finite element "truth" temperature field and velocity streamlines for $(\mathrm{Gr}, \phi) = (6000, 0)$ at (a) $t^k = 0.10$, (b) $t^k = 0.20$, and for $(\mathrm{Gr}, \phi) = (6000, 0.2)$ at (c) $t^k = 0.10$, (d) $t^k = 0.20$.

26   *D. J. Knezevic, N. C. Nguyen, A. T. Patera*

(a)   (b)
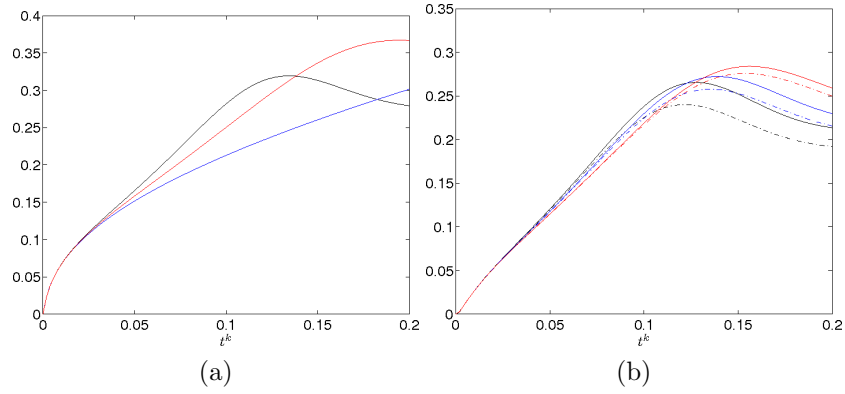
Fig. 3. (a) Truth output $s_2^{\mathcal{N}}(t^k; \mu)$ as a function of t^k for $(\mathrm{Gr}, \phi) = (6000, 0)$ (black), $(\mathrm{Gr}, \phi) = (3000, 0)$ (red), and $(\mathrm{Gr}, \phi) = (100, 0)$ (blue). (b) Truth outputs $s_1^{\mathcal{N}}(t^k; \mu)$ (dash-dot line) and $s_3^{\mathcal{N}}(t^k; \mu)$ (solid line) for $(\mathrm{Gr}, \phi) = (6000, 0.2)$ (black), $(\mathrm{Gr}, \phi) = (5000, 0.1)$ (blue), and $(\mathrm{Gr}, \phi) = (4000, 0.05)$ (red).

(a)   (b)
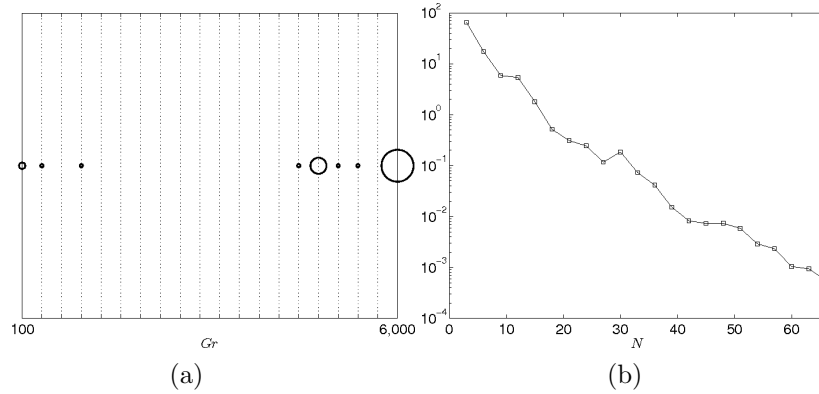
Fig. 4. Results of the POD-Greedy sampling procedure for the one-parameter problem: (a) the optimal parameter sample S^* — the frequency of a parameter value's occurence in S^* is proportional to the radius of the corresponding circle marker; (b) the convergence history of the maximum relative error $\epsilon_{N,\mathrm{max,rel}}^*$.
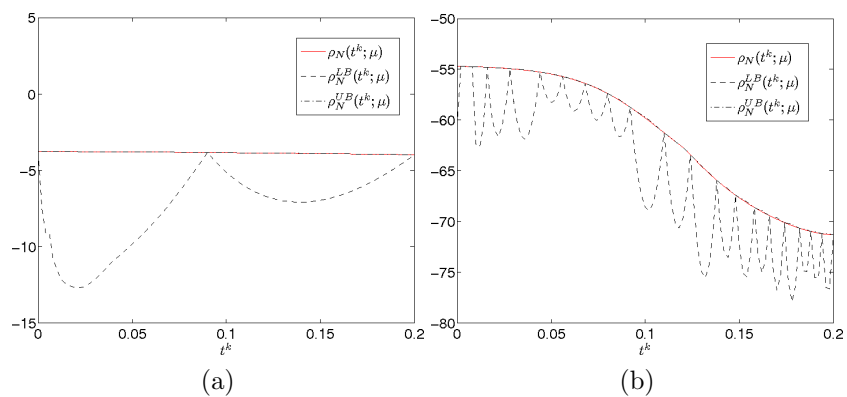
Fig. 5. Stability factor $\rho_N(t^k;\mu)$ as well as $\rho_N^{\mathrm{LB}}(t^k;\mu)$, and $\rho_N^{\mathrm{UB}}(t^k;\mu)$ — the SCM lower and upper bounds, respectively — as functions of t^k for $N = 66$: (a) Gr = 100, and (b) Gr = 6000.
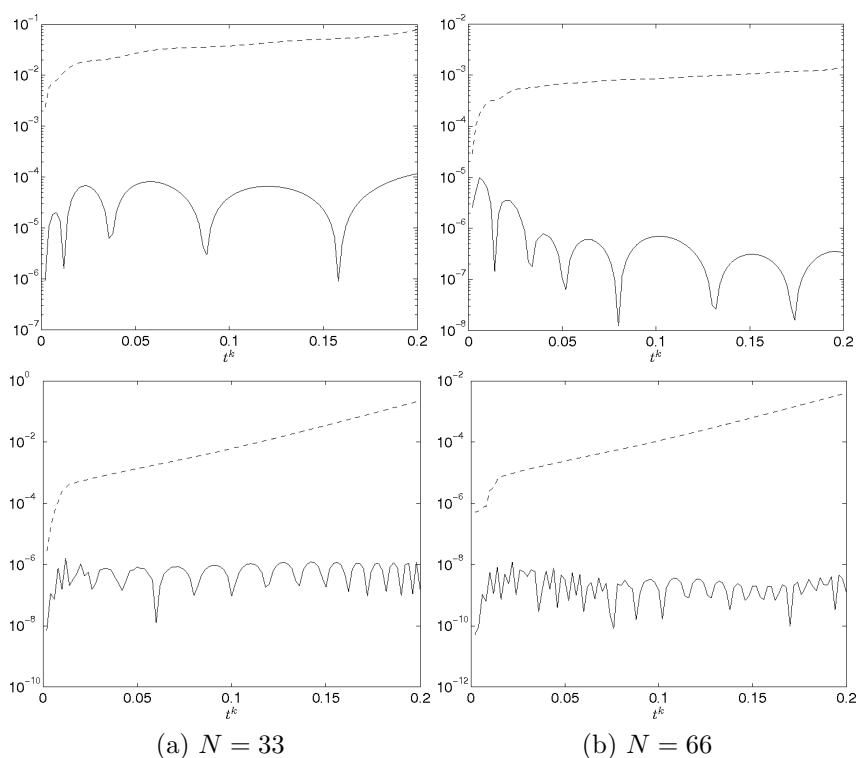

Fig. 6. The output error $|s_2^{\mathcal{N}}(t^k;\mu) - s_{N,2}(t^k;\mu)|$ (solid line) and error bound $\Delta_{N,2}^s(t^k;\mu)$ (dashed line) for this "middle" output as a function of t^k for (a) $N = 33$, and (b) $N = 66$: Gr = 100 (top row) and Gr = 6000 (bottom row).

28   *D. J. Knezevic, N. C. Nguyen, A. T. Patera*
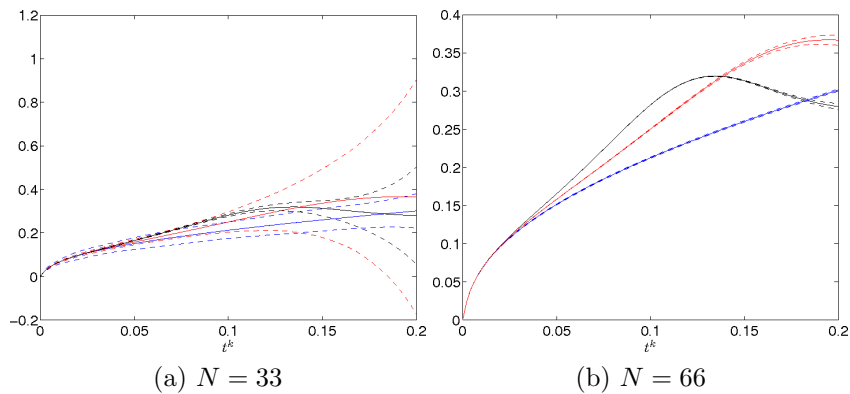

(a) $N = 33$ (b) $N = 66$

Fig. 7. The RB output $s_{N,2}(t^k; \mu)$ (solid lines) and corresponding error bounds $s_{N,2}(t^k; \mu) \pm \Delta^s_{N,2}(t^k; \mu)$ (dashed lines) as functions of t^k for (a) $N = 33$, and (b) $N = 66$: Gr = 100 (blue), Gr = 3000 (red), and Gr = 6000 (black).
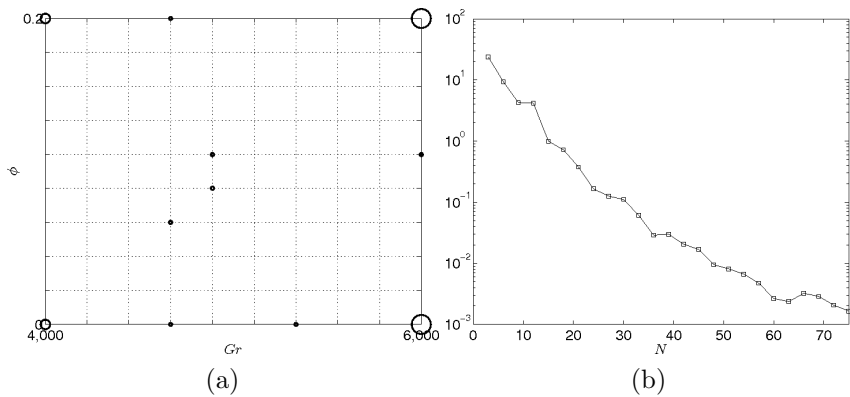

(a)   (b)

Fig. 8. Results of the POD-Greedy sampling procedure for the two-parameter problem: (a) the optimal parameter sample S^* — the frequency of a parameter value's occurence in S^* is proportional to the radius of the corresponding circle marker; (b) the convergence history of the maximum relative error $\epsilon^*_{N,\max,\text{rel}}$.
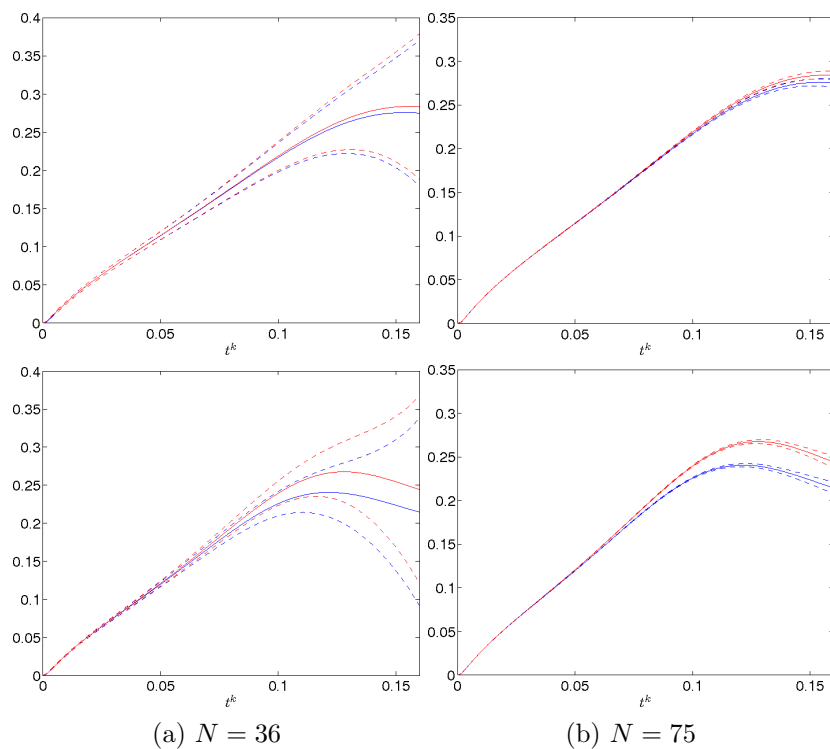
(a) $N = 36$ (b) $N = 75$

Fig. 9. The RB outputs $s_{N,1}(t^k; \mu)$ (blue, solid line) and $s_{N,3}(t^k; \mu)$ (red, solid line) and corresponding output bounds $s_{N,1}(t^k; \mu) \pm \Delta^s_{N,1}(t^k; \mu)$ (blue, dashed lines) and $s_{N,3}(t^k; \mu) \pm \Delta^s_{N,3}(t^k; \mu)$ (red, dashed lines) as functions of t^k for (a) $N = 36$, and (b) $N = 75$: $(\mathrm{Gr}, \phi) = (4000, 0.05)$ (top row) and $(\mathrm{Gr}, \phi) = (6000, 0.2)$ (bottom row).